A Reproduced Copy

OF

NASA CR-174,144

Princeton University

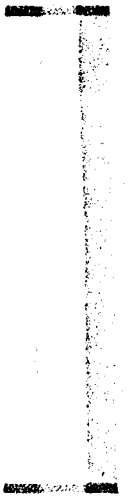

Department of Mechanical and Aerospace Engineering

STUDY OF THE STRUCTURE OF TURBULENT SHEAR FLOWS AT SUPERSONIC SPEEDS AND HIGH REYNOLDS NUMBER

Alexander J. Smits
Seymour M. Bogdonoff

Final Technical Report

NASA Grant NAGW-240

Covering the Period
September 1, 1981 thru August 31, 1984

Department of Mechanical & Aerospace Engineering
Gas Dynamics Laboratory
Princeton University
Princeton, NJ 08544

MAE 1690

December, 1984

TABLE OF CONTENTS

1. INTRODUCTION

This report is the Final Technical Report on NASA Grant NAGW-240, monitored by Drs. Clint Brown, Gary Hicks and Randolph Graves. The report describes experimental work on turbulent, supersonic shear layers performed at the Gas Dynamics Laboratory of Princeton University during the period September 1, 1981 to August 31, 1984.

The behavior of turbulent shear flows at high Reynolds numbers and supersonic speeds is of great practical interest, particularly in the internal and external aerodynamic design of aircraft. A good example is given by the flow through the compressor and turbine. Here, very complicated flows occur, and the boundary layers can experience severe adverse pressure gradients, interactions with shock waves, longitudinal curvature and possibly separation and reattachment. Similar observations can be made regarding the disturbances suffered by the external flow over the fuselage, wing and control surfaces.

Unfortunately, our present understanding of these complex flows is rather limited. As a result, the computations display severe shortcomings, and these inadequacies were well documented at the recent Stanford Conference on Complex Turbulent Flows (Kline, et.al. 1981). Consider the example shown in Fig. 1. Here, the calculations by Visbal and Knight (1983) are compared with the measurements by Settles, et.al. (1977) in four two-dimensional compression corner flows at Mach 3. The flows range from attached (8^{o}), to incipient separation (16^{o}) to separated (20^{o},24^{o}). The computer code was based on the Reynolds-averaged Navier-Stokes equations using the Baldwin-Lomax algebraic eddy viscosity model. As can be seen, the comparisons are not very favorable, especially for the higher corner angles and the results clearly demonstrate the inadequacy of the turbulence model.

For three-dimensional interactions, similar calculations have resulted in rather better agreement with experiment, at least in some cases. For example, Knight (1983) found good agreement between his calculations and the experimental study of a sharp fin interaction performed by Oskam (1976). Such calculations, however, require careful validation before they can be considered reliable and accurate. The recent computations by Horstman (1984) demonstrate how cautiously we must proceed. Horstman calculated a large number of swept compression corners, systematically varying the corner angle α and the sweepback angle λ. These results were compared with the experimental work by Teng and Settles (1982), Settles and Bogdonoff (1982) and Settles, et al. (1984), and Horstman found good agreement over a considerable range of α and λ. At high sweepback angles, however, sharp discrepancies occurred. In addition, the computations missed some important flow details at lower angles. Thus, computations can appear to be successful over some range of parameters and yet display severe shortcomings outside this range; without appropriate experimental work such discrepancies might pass unnoticed.

Experimental work, therefore, is required (i) to understand the physical mechanisms which determine the behavior of the flow, (ii) to develop improved turbulence models, and (iii) to generate data sets for the validation of computational work. In particular, we require further turbulence data; the existing measurements are scarce and generally of dubious quality (see, for example, Fernholz and Finley, 1981).

These needs were recognized by NASA, and the Gas Dynamics Lab was asked to begin a long range experimental program to study the behavior of turbulence in supersonic shear flows. We feel that this program has achieved major progress in the understanding and documentation of supersonic shear

layer behavior, and the current report summarizes our achievements. Further details are available from the publications produced under NASA sponsorship, and these are listed in Appendix A.

The research can be conveniently divided into three major areas: development and improvement of turbulence measuring techniques for supersonic flows (see Section 2); detailed experimental investigations of a limited number of flow geometries (Section 3), and development of physical models to explain the observed behavior of the flows (Section 4). In addition, a number of other activities took place which are not so easily classifiable, and these activities are described in Section 5. The conclusions are given in Section 6, together with some recommendations for future work.

2. INSTRUMENTATION DEVELOPMENT AND TESTING

Previous turbulence data displayed considerable scatter (see, for example, Fernholz & Finley, 1981), and a major effort was therefore undertaken to improve the accuracy of these measurements. Two techniques are available: hot-wire anemometry and laser-Doppler velocimetry. Early studies using the LDV technique (which requires seeding of the flow) showed that this method suffered from lack of resolution and seeding non-uniformity close to the wall and in strong velocity gradients. There was considerable doubt whether the particles followed the very sharp changes in flow direction which occur through such interactions. Our previous experience had shown that the hot-wire, with some restrictions, could be used for examining these flows, and our attention was therefore focussed on improving hot-wire techniques, and developing them to the point where hot-wires could be used to their full capability under the harsh conditions of supersonic tests.

In a blowdown facility such as the 8" x 8" supersonic channel at the Gas Dynamics Laboratory, run times are typically limited to one or two minutes. Such short run times make the use of conventional constant current hot-wire anemometers impractical. These anemometers require careful adjustment of the frequency response under actual operating conditions, and data acquisition is therefore rather slow. Thus, we have concentrated our efforts on improving constant temprature anemometer techniques. These systems compensate for frequency response automatically and considerably improve data acquisition efficiency. We have succeeded in developing reliable calibration and data acquisition techniques for normal and inclined wires operated in the constant temperature mode, and these methods have been reported at several conferences and in a number of archival journals (see Appendix A). To summarize, significant

original contributions in this area include the design of reliable and durable hot-wire probes, the analysis and experimental validation of inclined wire sensitivity in supersonic flow and the identification of the effects of normal Mach number, end conduction and wire bowing on inclined wire sensitivity. It was also shown, for the first time, that constant temperature systems display significant non-linearities at low overheat ratios, and they are therefore unsuitable for the measurement of temperature fluctuations. Only mass-flow fluctuations, $(\rho u)'$, can be satisfactorily measured with a constant-temperature system.

Two different probes were designed and tested: a normal wire probe, for measuring $(\rho u)'$, and an inclined wire probe, for measuring the mass-weighted Reynolds shear stress $\overline{(\rho u)'v'}$. The probes, and the calibration and testing procedures, are described briefly below.

2.1 Normal Wire Probe Design, Calibration and Testing

The current probe design is the result of considerable development. In our first design, bare tungsten wire was spot-welded to the prongs using a tungsten electrode. This proved to be highly unsatisfactory. Not only was the active wire length subjected to aerodynamic interference from the relatively bulky prongs, but it was also difficult to achieve a satisfactory bond between wire and prong, and wire breakages were very frequent. Instead, our current probe design closely follows that recommended by Kovasznay (1950). The tungsten wire (5 μm diameter) is first electroplated with copper and then soft-soldered to the prongs. A dilute suphuric acid solution is then used to etch away the copper coating and expose an active portion of tungsten wire approximately 0.8 mm long (Fig. 2). To avoid strain-gaging, a small amount of slack is usually introduced. This probe design drastically reduces wire breakage, and

in addition, minimizes the interference effect of the bow shocks emanating from the tips of the prongs (Figs. 3 and 4).

The probe was connected to a DISA 55M10 constant temperature anemometer. The overheat ratio was varied by changing the bridge resistance. The frequency response (deduced from a square-wave test) was optimized by adjusting the anemometer gain and filter setting. All wires were checked for strain-gaging, and those found to be suspect were discarded.

The anemometer output was separated into a mean and a fluctuating component by low- and high-pass filters each set at 10 Hz. The fluctuating component was digitized directly at 500 kHz sampling rate by a Preston Scientific GMAD-1 A/D converter, and the raw data was stored on-line in the memory of a Hewlett-Packard HP1000 minicomputer for further processing. The mean component of the output voltage was also recorded, along with other mean quantities, by a slower A/D converter.

The wires were tested and calibrated in a small Mach 3 pilot tunnel with a working section measuring 49.3 mm x 74.5 mm. The stagnation pressure was varied between 4×10^5 and 14×10^5 N/m^2 which, for a 5 μm wire, gave a wire Reynolds number range of approximately 80 to 250.

We demonstrated that the constant-temperature hot-wire anemometer is inherently unsuitable for measuring turbulent temperature correlations; the major reason is the non-linearity of the temperature sensitivity at low overheat ratios. The instrument is therefore restricted to measurements of the mass-flow fluctuations. If temperature fluctuations are present, high overheat ratios are desirable to avoid contamination of the mass-flow signal by contributions from the fluctuating temperature. Very high overheat ratios may be required if we wish to ignore these contributions entirely.

The maximum frequency response of the system depends on the anemometer roll-off frequency, the spatial resolution of the probe and the maximum A/D conversion rate. The maximum frequency response required depends on the experiment; all requirements on the frequency response become less stringent as the typical size of the shear layer increases.

It was found that the static calibration of the anemometer could be adequately represented by a modified King's Law. This calibration is a function of mean stagnation temperature and corrections are required to account for this dependence if the stagnation temperature varies with time, or with position in the flow field. The corrections were found to be significant, and a satisfactory correction procedure was suggested.

To demonstrate the constant-temperature hot-wire technique in practice, some measurements were made in the boundary layer developing on the tunnel floor of the Princeton University 203 mm x 203 mm Supersonic Wind Tunnel. The freestream Mach number was 2.9, the wall conditions were near-adiabatic, and the rms mass-flow turbulence level in the freestream was approximately 1%. The tunnel was operated at a stagnation pressure of 6.9×10^5 N/m^2, which gave a unit Reynolds number of 6.3×10^7/m. At the measuring position, the boundary layer thickness was about 26 mm, with a Reynolds number based on momentum thickness of 77,600.

Consider the data presented in Fig. 5. Figure 5a shows the mass-flow turbulence intensity as measured by three different wires, each operated at an overheat ratio of approximately 1.0. The repeatability of the measurements is obviously very satisfactory. The effect of varying the overheat ratio is demonstrated in Fig. 5b. Clearly, the data reach an asymptotic level as the overheat ratio increases, suggesting that the results taken at high overheat

are not significantly "contaminated" by total temperature fluctuations.

The inferred velocity fluctuation intensity is shown in Fig. 5c. The present measurements appear to be a little higher than most comparable data, particularly near the wall. The relatively high levels shown by our results may be due to the good spatial and temporal resolution of our measurements; significantly, our measurements agree well with the data of Johnson and Rose (1975) who used both LDV and hot-wire systems.

In conclusion, the overall trend shown by our data, and the level of quantitative agreement with previous data appears to be satisfactory.

2.2 Inclined Wire Probe Design, Calibration and Testing

The inclined wire probe design was similar to that used for the normal wire probe described in Section 2.1. The tungsten wire (5 μm diameter) was first electroplated with copper and then soft-soldered to the prongs. The central portion of the copper coating was etched away to expose an active portion of the tungsten wire approximately 0.8 mm long (see Fig. 6). For an inclined wire it is particularly important to isolate the central active length from the flowfield interference caused by the prongs, and the copper plated stubs served this purpose admirably (see Fig. 7). The angle formed between the mean flow direction and the normal to the wire for our probes was either 30°, or 45° (approximately).

The calibration facility, anemometer equipment and data analysis techniques were as described in Section 2.1. The inclined wire was calibrated for mass-flow rate sensitivity according to the procedure used for a normal wire. To calibrate the inclined wire for directional sensitivity, the probe was yawed through an angle of about $\pm 10^{\circ}$ from its null position using the device shown in Fig. 8. This device yaws the wire without changing its position in the flow.

We established a reliable calibration procedure for inclined wires operating in supersonic flow. The longitudinal mass-flow sensitivity at a fixed yaw angle was found by fitting a modified King's Law to the data. This data correlation was identical to that used in the analysis of normal wire data, with both correlations using an exponent $n = 0.55$. Several observations were made regarding the relative sensitivity ξ, defined as the ratio of the transverse to longitudinal mass-flow sensitivity (see Fig. 9). First, ξ appears to be independent of the Reynolds number. Second, although ξ depends strongly on the flow direction relative to the wire, the functional dependence is not simple; for instance, the cosine cooling law does not hold in supersonic flow. It seems best to find ξ by direct calibration. Third, when the relative sensitivity is a strong function of the yaw angle, the wire should be discarded to avoid errors due to nonlinearities. Fourth, in a supersonic flow ξ takes higher values than commonly encountered in subsonic flows.

The Mach number dependence of the inclined wire response was not investigated. Present indications are that this Mach number dependence is small, in agreement with the findings of Reshotko and Beckwith (1958). Further work on this question is currently in progress.

The calibration is a function of probe alignment and mean stagnation temperature. The corrections for temperature drift are similar to those used in the normal wire analysis. When the probe is misaligned by only a small amount, the senstivities may be corrected appropriately, but the measurements can not be interpreted without knowing the intensity of the longitudinal mass-flow rate fluctuations.

Two major restrictions limit the usefulness of the inclined wire in supersonic flow. The first restriction requires that the normal Mach number

must exceed 1.2. This places a limit on the maximum turbulence intensity that can be measured accurately. The second restriction is the necessity for a high system roll-off frequency. This lower limit on the frequency response is considerably higher than that required for normal wire measurements, and it may not be attainable in practice.

To demonstrate the inclined wire technique in practice, the mass-weighted Reynolds shear stress $\overline{(\rho u)'v'}$ was measured in a Mach 2.9 turbulent boundary layer. By comparing the results with corresponding data for similar flows, some indication of the measurement accuracy was obtained.

In these measurements, two different inclined wires were used, and the angle calibrations of these particular wires were those shown in Fig. 9. Both wires had a nominal diameter of 5 μm, a length-to-diameter ratio of approximately 180, and in each case the frequency response in the freestream was about 125 kHz. The boundary layer flow was typical of a zero pressure gradient layer, and the flow was identical to that investigated using normal wires. Further details of the flowfield, and the data acquisition system were given in Section 2.1.

The results are shown in Fig. 10. The Reynolds shear stress $\overline{u'v'}$ was deduced by assuming that (i) the pressure fluctuations were small, (ii) the total temperature gradient was small, and (iii) the turbulent Pradtl number was unity (Mikulla, in: Fernholz and Finley, 1981).

The normal Mach number restriction affects the measurements near the wall, and it will mean that $\overline{(\rho u)'v'}$ and $\overline{u'v'}$ are underestimated close to the wall. For a straight 30° wire in our Mach 2.9 boundary layer, the results are underestimated for $y/\delta < 0.1$ and for a straight 45° wire the results are underestimated for $y/\delta < 0.4$. When the wire is bowed, the situation is

considerably worse. For instance, with a bow of $\pm 10^{o}$, the results for a nominally 30^{o} wire are underestimated in the region $y/\delta < 0.2$, and a nominally 45^{o} wire cannot be used for $y/\delta < 0.6$. Thus the results for the two (slightly bowed) wires shown in Fig. 10 can be explained in terms of the normal Mach number criterion.

The $\overline{u'v'}$ measurements shown in Fig. 10b may be compared with the "best estimate" of the supersonic shear stress distribution suggested by Sandborn (1974). The agreement is rather poor for the 45^{o} wire, but the 30^{o} wire gives excellent agreement for $y/\delta > 0.2$. In fact, considering the size of the error bars, the agreement is rather better than expected. The discrepancies displayed by the 45^{o} wire for $y/\delta < 0.6$, and by the 30^{o} wires for $y/\delta < 0.2$ may be explained in terms of the normal Mach number criterion, as has already been discussed.

In practice, hot wires are often bowed, either because of thermal expansion; or because of a deliberate attempt to reduce strain-gauging effects. In addition to bowing, end-conduction effects may be responsible for the scatter observed in the directional sensitivity (see, for example, Fig. 9c).

The directional sensitivity of a bowed, inclined hot-wire was therefore investigated using a simple model for the convective heat transfer. The static response was analyzed for subsonic and supersonic flows. It was shown that the effects of both end conduction and wire bowing are greater in supersonic flow. Regardless of the Mach number, however, these two phenomena have distinctly different effects; end conduction apepars to be responsible for reducing the non-linearity of the response, whereas bowing increases the directional sensitivity (see Fig. 11).

It was also possible to calculate the temperature distribution along the bowed wire, and sample calculations are shown in Fig. 12. The effect of yaw on a straight wire is surprisingly small, and the temperature distribution is virtually unaffected by yaw angle. In contrast, the bowed wire temperature distribution is a strong function of yaw angle.

The position of the temperature peak occurs along the portion of the wire with the greatest sweepback, as may be expected. In addition, the maximum temperature for a bowed wire is considerably higher than the maximum for the straight wire. This observation has important consequences for hot wire filaments made of tungsten; to avoid oxidation the temperature at any part along the wire should remain below $600^{\circ}K$.

2.3 Current Development Work

Current development work in the area of hot-wire anemometry includes a micro-schlieren flow visualization investigation of the flow in the vicinity of the wire (preliminary results are shown in Figs. 4 and 7), the design of a suitable crossed-wire probe, the study of the hot-wire response in transonic flows and the development of a probe with an array of wires for the purpose of gathering data simultaneously at a number of points in the flow.

In addition to hot-wires, wall pressure transducers have been used in our lab for some time, particularly in the investigation of unsteady flows. Recently, we have extended the use of these transducers to multiple channels to measure space-time correlations, and to operate in combination with hot-wire probes to measure wall-pressure/velocity correlations. The validity of these measurements is restricted by the upper frequency response of the pressure transducers and the phase shift performance. These aspects are currently under investigation.

3. EXPERIMENTAL STUDIES

The hot-wire development resulted in a clear understanding of normal and inclined wire behavior, and it enabled us to take high quality turbulence measurements in supersonic flows. Great progress was achieved in using these hot-wire techniques to investigate a variety of interesting flows. These flows may be conveniently distinguished into two groups: shock-wave/boundary layer interactions produced by two-dimensional compression corners, and "isentropic compressions," where the boundary layer flows over a concavely curved surface. These flows were chosen to investigate the behavior of supersonic turbulent boundary layers in moderate to severe pressure gradients. In addition, the reattachment of a boundary layer separating off a backward-facing step was investigated in considerable detail to improve our understanding of the reattachment process. We will now consider each group of flows in turn, beginning with the reattachment study.

3.1 Reattaching Shear Layer Study

Using a backward facing step geometry, the incoming boundary layer was allowed to develop over a flat plate at Mach 2.9 before separating off the step and reattaching on a 20° ramp. The ramp was designed to eliminate the lip shock at the point of separation, and the separated flow formed a nominally self-preserving free shear layer without extraneous shocks and disturbances, and therefore it provided a well-defined initial condition for reattachment.

The test model is shown in Fig. 13. A turbulent boundary layer developed initially on the upstream flat plate (229 mm long). At the point where the boundary layer separated over a backward facing step, the boundary layer thickness δ_o was about 3.5 mm with a Reynolds number based on momentum thickness of approximately 14,000. The free shear layer, formed by the

separating boundary layer bridged a 25.4 mm deep cavity before reattaching on a plane ramp (see Fig. 14).

The flowfield steadiness was investigated by Settles et.al. (1983) using microsecond shadowgrams. In contrast to subsonic reattachment, where the reattachment line can move significantly, only a slight "tremble" of the wave system was observed. The magnitude of this wave motion was small compared to the average shear layer thickness and no large scale unsteadiness seemed to be present.

The upstream turbulent boundary layer separates without deflection at the corner of the backward facing step, forming a free shear layer. The shear layer mean velocity profiles achieve self-similarity at station SH43, which is approximately 17 δ_o downstream of the step. The growth of the shear layer is faster on the low-speed side than on the high-speed side, and, as a result, reattachment occurs at a point slightly below the geometric extension of the flat plate on the ramp surface. The static pressure rises before reattachment and continues to rise well downstream. The compression wave associated with the shear layer curvature coalesce to form a shock wave in the freestream, at some distance outside the shear layers.

Downstream of the mean reattachment point (station R27) a new boundary layer begins to develop. The adverse pressure gradient in this region gradually reduces and becomes negligible at about station R44. The mean velocity near the wall rapidly increases with downstream distance and the wall-layer thickness grows quickly. The velocity profiles initially display a very large wake component (as may be expected) but this soon decreases. By station R42, the mean velocity appears to dip below the standard logarithmic law, suggesting that the length scale near the wall is abnormally large. The relaxation of

the boundary layer is certainly not monotonic. For instance, both the Clauser parameter G and the wake parameter π reach high values near reattachment but undershoot their respective equilibrium values of 6.8 and 0.55 downstream. This behavior agrees with that observed in many subsonic reattachment studies (Bradshaw and Wong, 1972; Chandrsuda and Bradshaw, 1981).

The turbulence behavior is in some ways even more spectacular. Figure 15 shows the downstream evolution of the maximum rms mass-flow fluctuation intensity $\langle(\rho u)'\rangle$. In this figure, the turbulence intensities are normalized by the mean freestream mass flow upstream of the reattachment to show the amplification of the absolute intensity. To interpret the results in terms of the local freestream mass-flow rate, it may be noted that the freestream mass-flow rate increases by 97% through the compression. The arrows in Figs. 3 and 4 indicate the sonic point locations. The results below these points should be ignored, since the hot-wire calibration is not valid in the transonic and subsonic regions.

As can be seen, the fluctuation intensity in the free shear layer increases slowly with downstream distance. In contrast to the mean flow measurements, it appears that the turbulence intensity profiles do not achieve similarity at any stage before reattachment. However, this observation may be incorrect. The relative temporal and spatial resolution of the hot wire improves improves with increasing shear-layer thickness, and this may give the erroneous impression that the turbulence intensity is increasing.

The maximum turbulence intensity rises rapidly as the shear layer approaches the ramp, and at reattachment it reaches a level of almost 40% (see Fig. 15). Downstream of this point, the intensity continues to rise before reaching a maximum at station R42 (which coincides closely with the point where the static pressure gradient becomes negligible).

This large increase in turbulence level, persisting downstream of reattachment, is rather unexpected. In subsonic flow, downstream of a backward facing step, it has been observed that the turbulence level reaches a peak before reattachment and then decays rapidly. In contrast, in supersonic flow, we observe a dramatic amplification of the turbulence level. This experiment, therefore, clearly demonstrates the effect of compressibility on the turbulence behavior.

By using an approximate form of the turbulent kinetic energy equation, we demonstrated that mean dilatation significantly contributed to the amplification of the turbulence intensities. The overall flow behavior, however, was far from simple, and many competing influences were present. In particular, the turbulence length scale appeared to be both reduced by eddy bifurcation near reattachment and amplified by the action of extra strain rates due to dilatation and longitudinal curvature. In our analysis we ignored the possibility of turbulence amplification caused by unsteady oscillation of the wave system, and by local deformation of the compression waves by the turbulence itself. Several authors (Anyiwo and Bushnell, 1982; Zang et al., 1982) have suggested that these mechanisms may be important. In short, successful prediction of the present flow will require some very sophisticated modeling, and the challenge to the predictor is clear.

3.2 Compression Corner Studies

Three compression corners were surveyed using both normal and inclined wires. The corner angles were 8^{o}, 16^{o} and 20^{o}, which, at a Mach number of 2.9, correspond to a fully attached flow, a flow on the point of separation and a separated flow with a small separation bubble. The incoming flow was identical in all three cases, and the upstream boundary layer δ_o was approximately

26 mm thick, with a Reynolds number based on momentum thickness of 77,600. The results were reported in publications [1], [3], [12], [13] and [17] (see Appendix A), and the data were tabulated in publications [9], [14], [15] and [20]. These data compilations are particularly useful in disseminating results to computors (see Section 4), and we have adopted their production as standard practice.

The tunnel configuration is shown in Fig. 16. The tunnel was operated at a stagnation pressure of 6.9×10^5 N/m^2, and the unit Reynolds number was 6.3×10^7/m. The wall conditions were near-adiabatic and the freestream rms turbulence intensity was approximately 1%. The models were mounted on the tunnel floor and fitted with aerodynamic fences to avoid interference from the side-wall boundary layers. Blockage problems limited the model lengths downstream of the corner to 195 mm for the 8° model, 151 mm for the 16° model and 121 mm for the 20° model.

Constant temperature hot-wire anemometers were used throughout, and details of the operating procedure were given in Sections 2.1 and 2.2.

The normal wire measures fluctuations in mass-flow rate $(\rho u)'$. To determine the behavior of the fluctuations in velocity, we invoked Morkovin's (1962) "Strong Reynolds Analogy," which assumes that the pressure fluctuations are small, and that the density fluctuations are related to the velocity fluctuations according to

$$\frac{\langle \rho' \rangle}{\bar{\rho}} = (\gamma-1)\, M_a^2\, \frac{\langle u' \rangle}{\bar{U}}$$

These assumptions appear to hold even in severely perturbed boundary layers (see, for example Dussauge and Gaviglio, 1981). In addition to the above, the value of the density-velocity correlation is required. The measurements

by Dussauge and Gaviglio suggest a constant value of 0.8 across the boundary layer, and this value was adopted for all data analysis.

The inclined wire measures the mass-weighted shear stress $\overline{(\rho u)'v'}$. To determine the behavior of the turbulent shear stress $\tau = \overline{\rho u'v'}$, we again assumed that the "Strong Reynolds Analogy" could be applied. That is,

$$\tau/\tau_w = \frac{\bar{\rho}\,\overline{u'v'}}{\rho_w u_\tau^2} = \frac{2}{C_f}\,\frac{\bar{\rho}\,\bar{U}^2}{\bar{\rho}_{ref}\bar{U}_{ref}^2}\,\frac{1}{[1 + (\gamma-1)\,M_a^2]}\,\frac{\overline{(\rho u)'v'}}{\bar{\rho}\,\bar{U}^2}$$

where the subscript "w" indicates at the wall. In the case of the undisturbed, upstream boundary layer (see Fig. 17), the results agree closely with Sandborn's "best fit", which does not prove that the data are accurate, but nevertheless gives further confidence in our method.

Before presenting the turbulence measurements, it is useful to consider some aspects of the mean flow behavior.

The static pressure and skin friction coefficient distributions are shown in Figs. 18 and 19, respectively. From these figures, it is clear that the flow tends towards separation as the corner angle increases. In the 20° case, the flow has actually separated, with a separated zone approximately one-half δ_o long.

The mean velocity profiles generally demonstrate a quick recovery downstream of the corner. For all three cases, Settles, et al. (1979) observed that the profiles rapidly fill out and approach their equilibrium shape by the furthest downstream station.

3.2.1 Normal wire results

When we consider the turbulence behavior, however, it quickly becomes clear that the boundary layer is far from equilibrium, even at the furthest

point downstream. Figures 20 and 21 show the mass-flow fluctuation intensity $\langle(\rho u)'\rangle$ and velocity fluctuation intensity $\langle u'\rangle$. Note that the intensities are non-dimensionalized by the incoming freestream values $(\overline{\rho U})_{ref}$ and $\overline{U}_{ref}$. The figures therefore show the behavior of the absolute fluctuation levels.

The most obvious feature of the turbulence behavior is the dramatic amplification that occurs as the boundary layer passes through the interaction region. To understand this amplification more fully, it is useful to consider the evolution of the turbulence intensities along selected streamlines. In this way, the amplification may be related to the terms which appear in the Reynolds stress transport equations (see, for example, Hayakawa, et al., 1983).

Three streamlines, corresponding to upstream boundary layer locations of y/δ_o = 0.2, 0.4 and 0.6 were selected for this purpose (see Fig. 22). For each of these streamlines, the evolution of $\overline{u'^2}$, normalized by its upstream value is given in Fig. 23.

Figure 23 shows that these flows may be conveniently divided into two regions: an "interaction zone," which loosely corresponds to the region where severe pressure gradients exist, and a "recovery zone," which is the region downstream of the interaction zone. Within the interaction zone, $\overline{u'^2}$ displays a rapid increase along each streamline. The magnitude of the increase, however, is a function of both the initial position within the boundary layer and the shock strength; the largest increase occurs for the largest corner angle. In contrast, the behavior within the recovery zone does not display such a simple trend. Near the wall, the turbulence intensity decays quite rapidly (Fig. 23a), whereas further away the intensities are still increasing, even at the furthest downstream station (Fig. 23b). This behavior clearly reflects the time dependent response of the turbulent motions. As expected, the larger

eddies in the outer part of the boundary layer obviously respond more slowly than the motions near the wall.

3.2.2 Inclined wire results

The mass weighted Reynolds shear stress $\overline{(\rho u)'v'}/(\rho U^2)_{ref}$ is shown in Fig. 24. Before discussing these results, the accuracy and limitation of the hot-wire technique should be considered.

It is becoming increasingly clear that one of the major limitations on using inclined hot-wires in low Mach number supersonic flows is the requirement that the instantaneous normal Mach number should be greater than 1.2 (Smits and Muck, 1984). Within the transonic range, the hot-wire behavior changes drastically, and a sharp fall-off occurs in the inferred turbulence intensity. For this reason, results for which the normal Mach number is below 1.2 are expected to be in error and should be used cautiously although it may be possible to use the shear stress at the wall as a guide for interpreting the results near the surface.

Consider now the results shown in Fig. 24. The behavior of $\overline{(\rho u)'v'}$ is obviously rather different from that displayed by $\overline{(\rho u)'^2}$. For example, in passing through the interaction region, $\overline{(\rho u)'v'}$ for the 16° corner increases by as much as 16 times, whereas $\overline{(\rho u)'^2}$ increases by less than 10 times over the same distance. For the 20° corner, the maximum level at the last station is more than 20 times its upstream value. This may be compared to $\overline{(\rho u)'^2}$ which increased by about 16 times over the same distance.

The behavior of either the Reynolds stress $\overline{\rho}\,\overline{u'v'}$, or the kinematic shear stress $\overline{u'v'}$ may be deduced from the results for $\overline{(\rho u)'v'}$ by using the Strong Reynolds Analogy. Here we have chosen to present only the results for the kinematic stress $\overline{u'v'}$.

Figure 25 shows $\overline{u'v'}/\bar{U}^2_{ref}$ plotted against y/δ_o for the different streamwise stations. The behavior of $\overline{u'v'}/\bar{U}^2_{ref}$ is qualitatively similar to that of $\overline{u'^2}/\bar{U}^2_{ref}$. Quantitatively, however, the amplification of $\overline{u'v'}$ is not as great as that observed for $\overline{u'^2}$; this suggests that the turbulence structure is significantly changed through the interaction.

For instance, the ratio $-\overline{u'v'}/\overline{u'^2}$ can be taken as a structure parameter. In the undisturbed boundary layer at x = -51 mm, this ratio has a value of about 0.25 (at $y/\delta_o = 0.6$), which agrees well with the value commonly quoted for incompressible boundary layers (see Townsend, 1976, p.107). Through the interaction zone of the 16° corner, the ratio $\overline{u'v'}/\overline{u'^2}$ increases to about 0.32, although it must be stated that the measurements of $\overline{u'v'}$ in this region are probably not too reliable. Downstream in the recovery region, however, this ratio decreases significantly, and it reaches a value of 0.16 ∿ 0.18 at the furthest downstream station (x = 140 mm). A similar trend was observed by Smits et al. (1979) in a subsonic boundary layer subjected to an impulse in concave curvature. It is interesting to note that in the present experiment, where both curvature and compressibility effects are important, the turbulence appears to respond in a fashion similar to that observed in an incompressible curved flow.

In passing the interaction region of the 20° corner, however, $\overline{u'v'}/\overline{u'^2}$ drops by about 25%, and remains low, although it appears to recover slightly at the last two stations. This result contrasts distinctly with the behavior observed in the 8° and 16° corner studies: there the ratio increased sharply through the interaction before relaxing somewhat downstream.

3.2.3 Final discussion of compression corner flows

All turbulence quantities $\overline{(\rho u)'^2}$, $\overline{u'^2}$, $\overline{(\rho u)'v'}$ and $\overline{u'v'}$ show a qualitatively similar trend; all increase steeply on encountering the shock and continue to increase over a distance which corresponds approximately to the region of non-zero pressure gradient. The relaxation process downstream appears to be rather slow, and at the furthest downstream station (about 4 δ_o downstream of the corner), the turbulence is still far from equilibrium. Perhaps the most remarkable feature is that for the 20^o corner, the dimensionless turbulence structure parameter $\overline{u'v'}/\overline{u'^2}$ is significantly reduced in passing through the interaction, in contrast with behavior observed with 8^o and 16^o corner flows.

To interpret these results, we can begin by considering the theoretical work of Zang et al. (1982) and Anyiwo and Bushnell (1982). Using the two-dimensional Euler equations, these authors showed that several possible turbulence amplification or generation mechanisms may occur during an interaction between a plane shock wave and an incident turbulence field. These mechanisms include (1) direct amplification, (2) "generation" of turbulence from incident acoustic and entropy fluctuations, and (3) "focussing" caused by distortions of the shock front.

When a shock wave interacts with a turbulent boundary layer, however, the flow field is rather different from the ideal case considered by these authors. The shock wave within the boundary layer curves and is followed by a system of instantaneous compression waves (see, for instance, Fig. 3). All these waves are unsteady and appear to be in constant, low frequency motion (Dolling and Murphy, 1982). As Zang et al. (1982) point out, the direct conversion of mean flow energy into turbulence by shock oscillation

can serve as a powerful turbulence amplification mechanism.

For both the 8^{o} and 16^{o} corner flows, the effects of dilatation and curvature appeared to be sufficient to explain the measured amplification. Direct shock effects and shock oscillation did not seem to be overly important. This conclusion was supported principally by the behavior of the structure parameter $\overline{u'v'}/u'^2$. For example, Debieve et al. used an analysis based on rapid distortion theory to show that this parameter should increase through a shock, when the shock behaves as a stationary discontinuity. In addition, Smits, et al. (1979) found that $\overline{u'v'}/u'^2$ increased when a subsonic boundary layer was subjected to a short region of concave curvature. In the 20^{o} corner flow, however, this parameter decreased through the interaction. To explain this result, we tentatively suggest that shock oscillation may be important in this flow, in addition to the effects of dilatation and curvature. Shock oscillation is likely to become more important at these high corner angles because the strength of the shock increases and eventually produces separation. If the shock movement is essentially random, we expect that the mean flow energy is transferred more to the normal stresses rather than to the shear stresses. This explanation suggests that the motion of the shock wave generates significant "inactive" motions such as those discussed by Bradshaw (1967) in relation to highly retarded subsonic boundary layers.

3.3 Isentropic Compression Studies

We examined the evolution of the mean flow and the turbulent stresses in a supersonic boundary layer experiencing the effect of bulk compression and streamline curvature. This study was prompted in part by the investigations of shock-wave/boundary layer interactions generated by two-dimensional compression corners (see Section 3.2). In that work, it was observed that

the boundary layer parameters suffered considerable distortion; in particular, the turbulent stresses were dramatically amplified. Four separate mechanisms for turbulence amplification were identified: "direct" amplification by the shock wave oscillation; the destabilizing effect of compression downstream of the shock, and the destabilizing effect of concave curvature.

The present investigation was designed to isolate the effects of compression and curvature. Instead of turning the flow suddenly, as in a compression corner, the turning was accomplished more gradually, through a short region of concavely curved wall. By spreading the pressure rise over several boundary layer thicknesses, the shock wave forms outside the boundary layer and it has no direct effect on the boundary layer behavior.

The incoming boundary layer and upstream flow conditions were identical to those used in the compression ramp studies. The upstream boundary layer was allowed to develop fully under a nominally zero pressure gradient on the wind tunnel floor before entering a short region of surface curvature. Just upstream of the curved wall, the boundary layer thickness δ_o was approximately 26 mm. The total turning angle was fixed at 8^o. Two different constant radii curvatures were investigated: the first had a radius of 254 mm, the second a radius of 1270 mm. These correspond to ratios of δ_o/R of approximately 0.1 and .02 respectively. Both curvatures were followed by a short (153 mm) recovery region, allowing us to study the initial relaxation behavior of the boundary layer (see Fig. 26).

The mean flow behavior for both models was previously reported by Taylor and Smits (1984) and Taylor (1984). Briefly, the velocity profiles displayed a "dip" below the log-law, suggesting an increase in the turbulence length scale, and no evidence was found for the presence of longitudinal

roll-cells, as might be expected to occur in concavely curved shear layers. In both these respects, the flow was similar to the incompressible flow studies by Smits et al. (1979), who investigated the response of a boundary layer as it experienced the combined effects of concave curvature and lateral divergence. In the present flow, the boundary layer experiences the combined effects of concave curvature and bulk compression, and the analogy between divergence and compression, first suggested by Green in Bradshaw (1973), was strengthened considerably by these mean flow observations.

Measurements of the turbulence behavior were also taken. Normal and inclined hot-wires were used, and the measurements describe the behavior of the longitudinal mass-flow fluctuations $(\rho u)'$ and the mass weighted shear stress $\overline{(\rho u)'v'}$. The kinematic stresses $\overline{u'^2}$ and $\overline{u'v'}$ were deduced using Morkovin's "Strong Reynolds Analogy." Wherever possible, the results for the 8^{o} compression corner were compared with those for Models I and II. The incoming boundary layer and the upstream freestream conditions were identical in all three experiments. The static pressure and skin friction distributions are compared in Figs. 27 and 28, respectively, and the figures demonstrate that the experiments cover a wide range of stress gradients, that is, a wide range of strain rates, although the overall pressure rise and turning angle are the same in each case. Hence, these experiments investigate, for a given perturbation strength, the effect of varying perturbation rate.

The variation of the longitudinal component of the turbulence intensity is shown in Fig. 29. The upstream reference conditions were used as non-dimensionalizing variables throughout, and hence the results show the behavior of the absolute turbulence levels.

The general behavior of $\overline{u'^2}$ is very similar in all cases. Initially, there is a rapid amplification of $\overline{u'^2}$ through the perturbation zone. This increase continues further downstream, and the peak amplification of $\overline{u'^2}$ is about three-fold in each case. In the outer part of the boundary layer, there is little sign of any recovery or relaxation but near the wall the intensities quickly fall, indicating that the relaxation process begins at the wall and propagates outward.

The variation of the kinematic shear stress $\overline{u'v'}/U^2_{ref}$ is shown in Fig. 30. Again, a considerable amplification occurs through the perturbation zone, continuing into the region downstream, and the relaxation appears to propagate outwards from the wall. However, the peak amplification levels for the three cases differ considerably; for the compression corner and Model I it is about four-fold, whereas for Model II it is only about two-fold.

Hence, the present results show that structure parameters, such as $\overline{u'v'}/\overline{u'^2}$, are clearly a function of the perturbation rate.

As far as the turbulence behavior is concerned, the compression corner and Model I influence the turbulence in an almost identical manner. This result suggests that the perturbation in these two cases is sufficiently rapid to alter the turbulence in a manner which depends only on the overall changes that occur, not on the path taken. The parameter describing this "change of state" is therefore the total strain, that is, the integral of the strain rate over the time it acts. For the curvature, this integral is equal to the total turning angle, and for the compression it is equal to $(1/\gamma)\ell n(p_2/p_1)$. It appears that the shock wave itself has no explicit effect on the turbulence but this conclusion can only hold if the shock is relatively weak, such that the entropy loss is small, and separation with the concommitant

unsteadiness is avoided. This condition seems to be satisfied in the 8^{o} compression corner experiment.

The response of the turbulence to the perturbation produced by Model II is quite different to that seen in the other two experiments. For example, the stress ratio $\overline{u'v'}/\overline{u'^2}$ is affected by only a relatively small amount. Hence, despite the large amplification of the absolute turbulent stresses, the turbulence structure is not radically altered, implying that the perturbation is sufficiently slow for some redistribution processes to occur. In this case, the local strain rates are probably more useful than the total strain for describing the response of the turbulence. The results from this particular experiment, therefore, appear to constitute an excellent test case for developing turbulence models.

Close to the wall, we observed the beginning of a relaxation process in all three experiments. It is to be expected that the flow near the wall will attain equilibrium more quickly than the flow in the outer part of the layer; a measure of the large eddy time constant is the turbulent energy divided by its rate of production, and this will vary approximately as $1/(\partial U/\partial y)$ (Bradshaw, 1973). This relaxing region grew in size as we proceeded downstream, and its growth resembled that of a new boundary layer. Similar "internal layers" have been observed in boundary layers perturbed by sudden changes in surface roughness, surface curvature, and pressure gradient (Smits and Wood, 1985) and the similarity displayed by the propagation of the relaxation outward from the wall may be useful in a qualitative understanding for the flow behavior in the present experiments.

3.4 Summary and Conclusions of Experimental Work

When taken as a whole, the experimental work leads to several interesting conclusions. For example, we have seen that turbulence levels are strongly amplified in a shock-wave boundary layer interaction. This amplification appears to be caused by direct, virtually inviscid amplification across the shock, followed by the combined effects of adverse pressure gradient, compressive extra strain-rates and concave curvature. When the shock strength is relatively low (that is, no separation occurs) it seems that the important parameter is the overall pressure rise rather than the presence of a shock-wave. This was demonstrated by the results from the isentropic compression studies. When the shock strength increases, however, shock-wave oscillation becomes an important amplification mechanism. Here, mean flow energy is directly transferred into unsteady turbulent motions. This process is apparently random, and therefore contributes more to the random motions which increase the total turbulent energy than to the organized motions associated with the shear stresses. This hypothesis explains why the structure parameter $\overline{u'v'}/\overline{u'^2}$ increases through the interaction for the 8° and 16° compression corners, and decreases for the 20° compression corner; when the flow separates at higher angles, shock-wave oscillation becomes important.

4. ANALYTICAL AND COMPUTATIONAL WORK

Throughout the period of our previous funding, we have maintained close contact with several computational groups, especially those groups headed by Prof. D. D. Knight at Rutgers University, and Dr. C. C. Horstman at NASA-Ames. In addition, our contacts include R. E. Melnik (Grumman Aerospace Corporation), Ha Minh Hieu (l'Institut National Polytechnique de Toulouse), D. Degani (Technion), J.-P. Bonnet (Poitiers) and H. H. Legner (Physical Sciences, Inc.). All of these groups have expressed interest in trying to calculate the compression corner flows, although they generally use rather conventional turbulence models.

What is perhaps more promising is the approach suggested by Dussauge and Gaviglio (1981), Debieve et.al. (1982) and Anyiwo and Bushnell (1982). In this work, the concept of "sudden distortion" is applied to compressible flows experiencing a short region of intense pressure gradient, including the interaction with a shock-wave. When the perturbation is sudden, that is, the perturbation occurs over a time which is considerably less than the response time of the turbulent motions, then the distortion may be essentially inviscid. The turbulent motions are then affected only through the distortion of the mean field, and nonlinear effects caused by turbulence-turbulence interaction can be neglected. This approach appears to have considerable promise in calculating the turbulence behavior observed in our experimental work. We have been fortunate enough to have had Dr. J.-P. Dussauge from I.M.S.T. in Marseille as a Visiting Research Fellow this year, and we are working closely with him to complete the calculation of our compression corner flows as well as the "isentropic" compressions. Preliminary work suggests that this essentially inviscid analysis might supplement more conventional schemes,

PAGE 30 IS MISSING
FROM ORIGINAL

5. MISCELLANEOUS ADDITIONAL WORK

Earlier this year, Professor H. Fernholz from the University of Berlin spent six weeks in the Laboratory as a Visiting Research Fellow. During this period, we had the opportunity to interact closely with him, and we intend to maintain these discussions in the future. In particular, we are making our data available to him for future publication in AGARDograph form.

In another development this year, Professor A. Smits of the Gas Dynamics Laboratory was invited to write a review article for Annual Reviews of Fluid Mechanics. Entitled "The response of turbulent boundary layers to a sudden perturbation," the article is co-authored with Dr. D. H. Wood from Newcastle University (Newcastle, Australia), and is due to appear early in 1985.

6. PROPOSALS FOR FUTURE WORK

The conclusions and observations from our previous work lead us to propose the following. Firstly, we are interested in testing our current understanding of shock-wave boundary layer interactions. Although we have identified some of the important physical mechanisms, we are still far short of a quantitative understanding. Further theoretical and experimental work is required to produce a useful turbulence model. In the experiments performed thus far, many different effects were acting simultaneously. To understand these effects fully, we need to study them in isolation, and our first priority is to investigate relatively simple geometries such as a flat plate boundary layer subjected to a severe adverse pressure gradient. In this geometry, the effects of the shock, as well as effects of the curvature would be eliminated. Preliminary work has already commenced, and we have designed models to reproduce on a flat plate the pressure gradients observed in the isentropic compression corners. By comparison between these sets of experiments, we will be able to distinguish between the effects of compression and curvature. In a complementary study, we propose to complete the isentropic compression work by investigating a flow with a total turning angle of 16^{o} and $\delta_o/R = 0.02$. This work will provide important information on the range of applicability of Rapid Distortion Theory. The model has already been constructed, and the mean flow studies have been completed (publication [22], Appendix A), although the turbulence measurements have not yet commenced.

In addition, we are interested in studying the time-dependent behavior of turbulent motions in a supersonic boundary layer. We feel that this work is essential to a proper understanding of turbulent transport properties, and

it will represent a significant departure from our previous work which used the more conventional approach based on Reynolds-averaged quantities.

We propose to begin with a detailed study of the 24^{o} corner at Mach 2.9. Here, a substantial separated region exists, and shock-wave oscillation is expected to be particularly important. Currently, Drs. K. C. Muck and J.-P. Dussauge are measuring the correlation between wall pressure and velocity fluctuations. These measurements will provide information regarding the "inactive" motions, and the data should test our suggestion that shock-wave oscillation amplifies the random motions more than the organized motions. In this study, we have also used an array of four wall pressure transducers to study space-time correlations of the pressure signal and the distribution of phase velocities. Preliminary results indicate that the shock-wave oscillation displays both a bulk motion backwards and forwards as well as a spanwise wrinkling effect. We propose to complete the analysis of existing data and to extend the experimental work. In this work, we propose to begin with a set of conditionally sampled measurements wehre the shock wave position is used as a trigger for the conditional sampling. In this way, the instantaneous conditions before and after the shock wave can be determined. We also propose <u>active</u> control of the shock wave position by applying a perturbation to the separation bubble. By controlling the shock wave motion, the effect of shock wave oscillation may be more clearly defined. To study the instantaneous wall conditions, an array of thin hot-film gauges will be mounted flush with the wall. These gauges will provide instantaneous wall shear information, and will enable us to discern the connection between the shock wave motion and the behavior of the separation bubble.

On a more fundamental level, we propose a detailed study of the large-scale motions in a flat plate zero pressure-gradient boundary layer. A great

deal of work has been performed to identify the characteristic motions, sometimes called coherent structures, which occur in turbulent shear flows, but our current understanding of these large-scale motions is mainly derived from subsonic flow studies at relatively low Reynolds number (see, for example, Brown & Thomas, 1977). We propose to use multiple hot-wires, combined with arrays of flush-mounted hot films, to similarly characterize the nature of a compressible , high Reynolds number boundary layer. We believe that this study would be the first of its kind. Some work has already commenced in this area, although the measurements thus far have been confined to mapping out the overall nature of the boundary layer. By measuring $\overline{uv}$ and $\overline{uw}$ in the spanwise and streamwise directions, we have established that the boundary layer is acceptably uniform and two-dimensional. Preliminary measurements of the wall pressure-velocity correlations are currently being analyzed.

In another major effort, we propose to examine the relaxation behavior of the boundary layer far downstream of a severe perturbation such as an interaction with a shock wave. This behavior is of great practical interest. For example, as the flow enters an inlet, the boundary layers interact with the entry shock system and then relax before entering the compressor stage. Thus, it is the relaxation behavior which really governs the engine inlet condition. The relaxation process is highly nonlinear, however, and very difficult to calculate. It is also experimentally difficult, and no measurements are currently available far downstream. In our present facility, such measurements are not possible but our new facility (funded by a recent DOD equipment grant, see Appendix C), will allow this work to proceed. This facility features a flexible diffuser, which by careful adjustment will create a relatively long disturbance-free region downstream of the interaction ($\geq 50\ \delta_o$).

We propose to begin with a study of the relaxation behavior downstream of an 8^{o} compression corner. In terms of turbulence modelling, our ultimate aim is to combine a rapid distortion analysis for the interaction region with a suitable transport model (such as a k-ε model, for example) to describe the relaxation process.

As support for the work mentioned above, we intend to modify existing instrumentation and develop and test a variety of new instruments. The proposed work in hot-wire anemometry, and in the measurement of wall pressure fluctuations has already been mentioned. In particular, we wish to develop a hot-wire rake capable of taking velocity data simultaneously at a number of points within the boundary layer. We have also alluded to flush-mounted thin-film gages for the measurement of instantaneous wall shear stress. These gages were suggested by Prof. Nosenchuck of our Department, and have the potential to measure the mean and fluctuating skin-friction, $\overline{\tau_w} + \tau_w'$.

Several other techniques are being developed within the Laboratory, with particular emphasis on new and improved flow visualization methods. Our long-range goal is to visualize the whole flowfield and its behavior as a function of time, with sufficient resolution to examine detailed areas of the flow. We have identified many possible techniques, including sharp-focus schlieren, multiple schlieren, tracing "hot-spots" generated by spark discharges or high-energy laser pulses, multiple high-speed imaging techniques and local vapor screen methods.

We are also continuing our development of the Resonant Doppler Velocimeter (RDV) as a flow visualization tool. Here, the fluorescence of an atomic or molecular seeding species is used to highlight areas of high or low velocity, temperature and pressure (see Zimmerman and Miles 1983 and Zimmerman et al. 1983).

In the long term, the RDV techniques will allow quantitative analysis of mean and fluctuating pressure, velocity and temperature within the flow field (Cheng et al. 1983). In the short term, however, we feel that another technique is required to supplement (and cross-check) the hot-wire measurements. We expect, therefore, to begin laser-Doppler measurements within the next three years. This will require considerable development, plus capital investment, and we hope to find support for this work.

One of our primary purposes in pursuing this experimental work is to develop a quantitative model for the turbulence behavior in compressible boundary layers. We propose to begin this task by (a) extending the work performed by Bradshaw on small extra strain rates and impulsively applied extra strain rates, and (b) modifying the rapid distortion approach suggested by workers at the Institut de Mechanicque de la Turbulence at Marseille. In addition, the effect of shock wave oscillation will be examined by extending the work of Anyiwo and Bushnell (1982) and the work of Debieve et.al. (1982). We feel that these inviscid approaches to suddenly perturbed flows hold great promise, and we anticipate making substantial progress in this area.

REFERENCES

1. Anyiwo, J.C., Bushnell, D.M., 1982. Turbulent Amplification in Shock-Wave Boundary Layer Interaction, AIAA J. 20:893-99.

2. Bradshaw, P., 'Inactive' Motion and Pressure Fluctuation in Turbulent Boundary Layers, Journal of Fluid Mechanics, V30, pp. 241-58.

3. Bradshaw, P. and Wong, F.Y.F., The Reattachment and Relaxation of a Turbulent Shear Layer, Journal of Fluid Mechanics, Vol. 52, 1972, pp. 113-135.

4. Bradshaw, P., (1973): Effects of Streamline Curvature on Turbulent Flow. AGARDograph 169.

5. Bradshaw, P., (1974): The Effect of Mean Compression or Dilatation on the Turbulent Structure of Supersonic Boundary Layers, J. Fluid Mech. 63, 449.

6. Brown, G.L., Thomas, A.S.W., 1977. Large Structure in a Turbulent Boundary Layer, Phys. Fluids 20:

7. Chandrsuda, C., and Bradshaw, P., Turbulence Structure of a Reattaching Mixing Layer, Journal of Fluid Mechanics, Vol. 110, 1981, pp. 171-194.

8. Cheng, S., Zimmerman, M., and Miles, R.B., 1982. Separation of Time-Averaged Turbulence Components by Laser-Induced Flourescence, Phys. Fluids 26:874-77.

9. Debieve, J.-F., Gouin, H. and Gaviglio, J., 1982. Evolution of the Reynolds Stress Tensor in a Shock-Wave Turbulence Interaction, Ind. J. Tech. 20:90-97.

10. Dolling, D.S., Murphy, M., (1982): Wall Pressure in a Supersonic Separated Compression Ramp Flow Field. AIAA Paper 82-0986.

11. Dussauge, J.P. and Gaviglio, J., 1981. Bulk Dilatation Effects on Reynolds Stresses in the Rapid Expansion of a Turbulent Boundary Layer at Supersonic Speed, Proc. Third Symp. on Turbulent Shear Flows, Univ. Cal. Davis, pp. 2.33-38.

12. Fernholz, H.H. and Finley, P.J., 1981. A Further Compilation of Compressible Boundary Layer Data with a Survey of Turbulence Data, AGARDograph 263.

13. Hayakawa, K., Smits, A.J. and Bogdonoff, S.M. (1981), Turbulence Measurements in a Compressible Reattaching Shear Layer, AIAA Paper 83-0299.

14. Johnson, D.A., Rose, W.C., 1975: Laser Velocimeter and Hot-Wire Anemometer Comparison in a Supersonic Boundary-Layer, AIAA Journal 13, 512-515.

15. Kline, S.J., Cantwell, B.J. and Lilley, G.M., 1981. Proc. 1980-81 AFOSR-HTTM-Stanford Conference on Complex Turbulent Flows: Comparison of Computation and Experiment, Thermosciences Division, Mech. Engrg. Dept., Stanford Univ., Stanford, CA.

16. Knight, D.D., 1983. A Hybrid-Explicit Numerical Algorithm for the Three-Dimensional Compressible Navier-Stokes Equations, AIAA Paper 83-0223.

17. Kovasznay, L.S.G., 1950: The Hot-Wire Anemometer in Supersonic Flow, J. AeroSciences 17, 565-573.

18. Morkovin, M.V., 1962, Mecanique de la Turbulence. Favre, A., Ed., C.N.R.S., Paris, pp. 367-380.

19. Oskam, B., 1976. Three-Dimensional Flowfields Generated by the Interaction of a Swept Shock Wave with a Turbulent Boundary Layer, Princeton Gas Dynamics Laboratory, Report #1313.

20. Reshotko, E. and Beckwith, I.E., Compressible Laminar Boundary Layer Over a Yawed Infinite Cylinder with Heat Transfer and Arbitrary Prandtl Number, NACA Report 1379, 1958.

21. Sandborn, V., 1974. A Review of Turbulence Measurements in Compressible Flow, NASA TMX-62337.

22. Settles, G.S., 1975. An Experimental Study of Compressible Turbulent Boundary Layer Separation at High Reynolds Numbers. Ph.D. Thesis, Aerospace and Mechanical Sciences Dept., Princeton University, Princeton, NJ.

23. Settles, G.S. and Bodgonoff, S.M., 1982. Scaling of Two- and Three-Dimensional Shock/Turbulent Boundary Layer Interactions at Compression Corners, AIAA Jour., pp. 782-789.

24. Settles, G.S., Fitzpatrick, T. and Bogdonoff, S.M., 1977. Detailed Study of Attached and Separated Compression Corner Flowfields in High Reynolds Number Supersonic Flow, AIAA J. 17:579-585.

25. Settles, G.S., Baca, B.K., Williams, D.R. and Bogdonoff, S.M., Reattachment of a Compressible Turbulent Free Shear Layer, AIAA Journal, V20, pp. 60-67, 1982.

26. Settles, G.S., McKenzie, T.M. and Horstman, C.C., 1984. Flow Field Scaling of a Swept Compression Corner Interaction - A Comparison of Experiment and Computation, AIAA Paper 84-0096.

27. Smits, A.J., Young, S.T.B., Bradshaw, P., 1979: The Effect of Short Regions of High Surface Curvature on Turbulent Boundary Layers, J. Fluid Mech. 94:209.

28. Smits, A.J., Hayakawa, K., Muck, K.C., 1983: Constant Temperature Hot-Wire Anemometer Practics in Supersonic Flows. Part I: The Normal Wire. Experiments in Fluids 1:83.

29. Smits, A.J., Much, K.C., 1983: Constant Temperature Hot-Wire Anemometer Practice in Supersonic Flows. Part II: The Inclined Wire. Experiments in Fluids 2:33.

30. Smits, A.J. and Wood, D.H., 1985. The Response of Turbulent Boundary Layers to Sudden Perturbations, Ann. Rev. Fluid Mech. 17:321-58.

31. Taylor, M.W. and Smits, A.J., 1984. The Effects of a Short Region of Concave Curvature on a Supersonic Turbulent Boundary Layer. AIAA Paper 84-0169.

32. Taylor, M.W., 1984. A Supersonic Turbulent Boundary Layer on Concavely Curved Surfaces, MAE Report 1684, Dept. Mechanical and Aerospace Engineering, Princeton University, Princeton, N.J.

33. Teng, H.Y. and Settles, G.S., 1982. Cylindrical and Conical Upstream Influence Regimes of 3-D Shock/Turbulent Boundary Layer Interactions. AIAA Paper 82-0987.

34. Townsend, A.A.: The Structure of Turbulent Shear Flow. Cambridge University Press, 1976.

35. Visbal, M.R. and Knight, D.D., 1983. Evaluation of the Baldwin-Lomax Turbulence Model for Two-Dimensional Shock Wave Boundary Layer Inter-Actions. AIAA Paper 83-1697.

36. Zang, T.A., Hussaini, M.Y., and Bushnell, D.M., Numberical Computations of Turbulence Amplification in Shock Wave Interactions. AIAA Paper 82-0293, 1982.

37. Zimmerman, M., Cheng, S. and Miles, R.B., 1983. Velocity Selective Flow Visualization in a Free Supersonic Nitrogen Jet with the Resonant Doppler Velocimeter, Proc. Third International Symp. on Flow Visualization, University of Notre Dame, Indiana.

38. Zimmerman, M. and Miles, R.B., 1983. Spatially Resolved Flow Visualization of a Wake Using Laser Induced Flourescence, Proc. Third International Symp. on Flow Visualization, University of Notre Dame, Indiana.

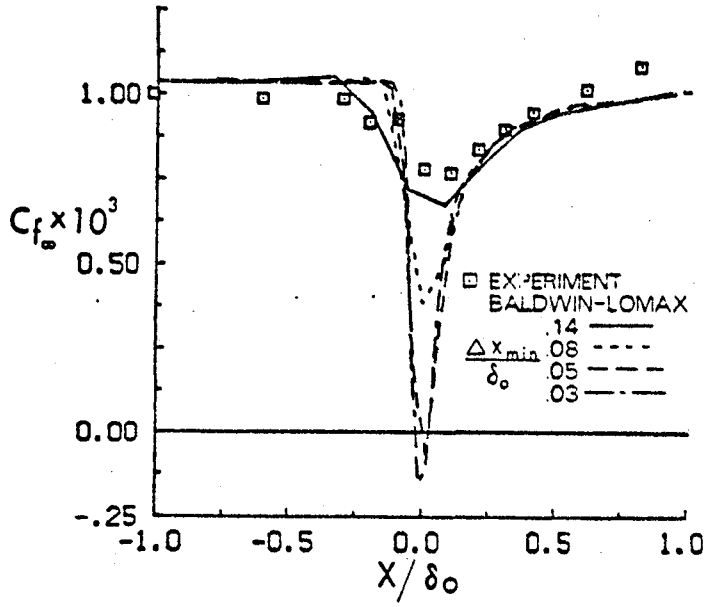

Skin friction coefficient for 8° ramp (Re_{δ_o} = 1.6 x 10^6).

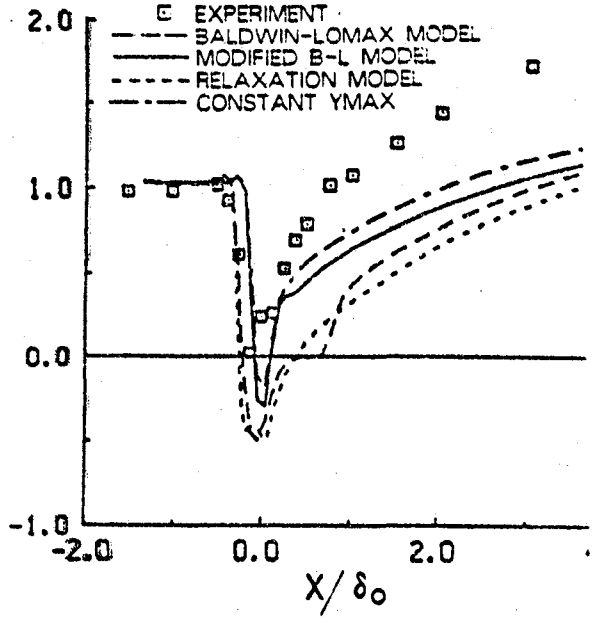

Skin friction coefficient for 16° ramp (Re_{δ_o} = 1.6 x 10^6).

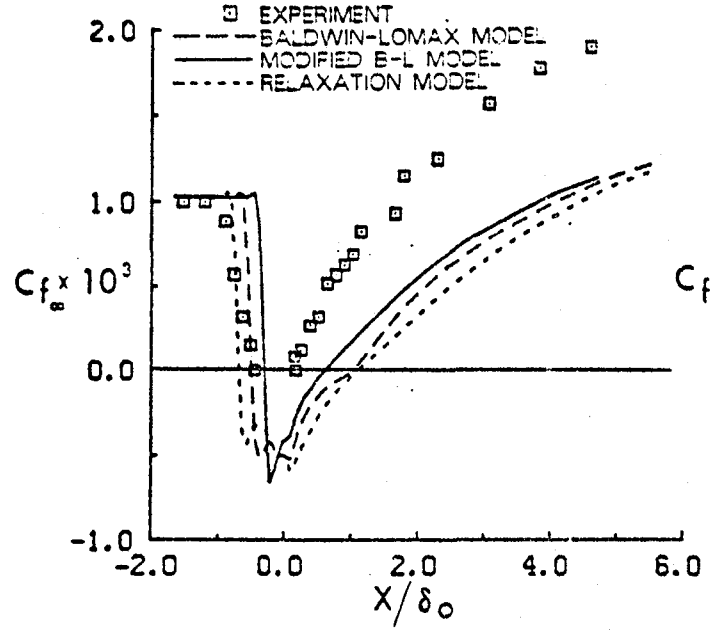

Skin friction coefficient for 20° ramp (Re_{δ_o} = 1.6 x 10^6).

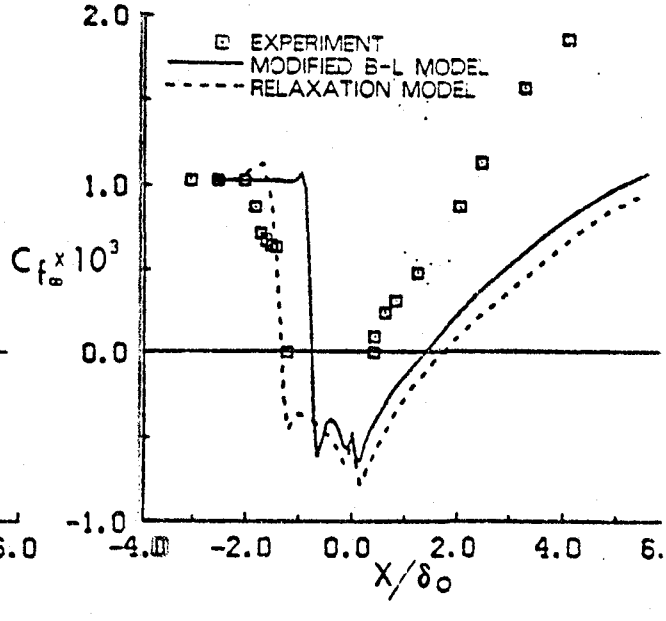

Skin friction coefficient for 24° ramp (Re_{δ_o} = 1.6 x 10^6).

Figure 1. Comparison between experiment (Settles et. al 1978) and computation (Visbal and Knight 1983) for compression corner flows.

Fig. 2 Sketch of current probe design. Wire is tungsten, 2 to 5 μm diameter, 0.8 mm long.

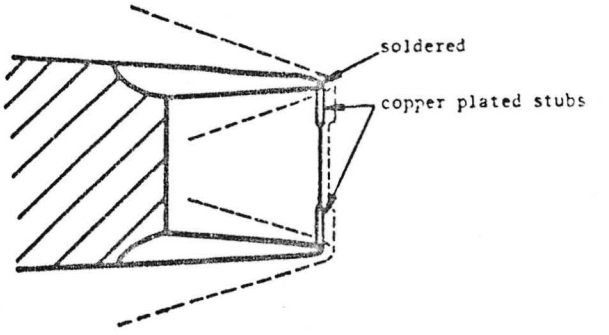

Fig. 3 Detail of probe design, showing approximate shock locations. (Major shocks only.)

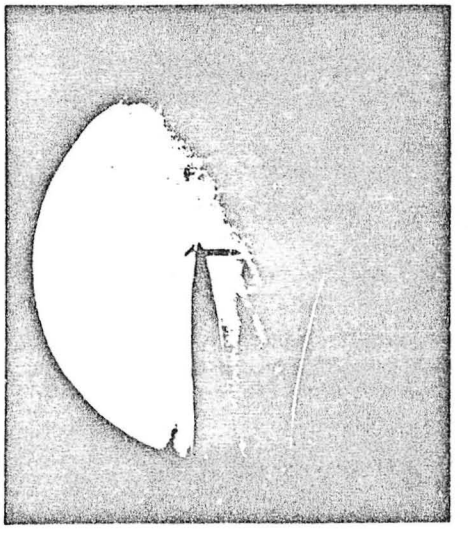

Fig. 4. Microschlieren photograph of normal wire probe.

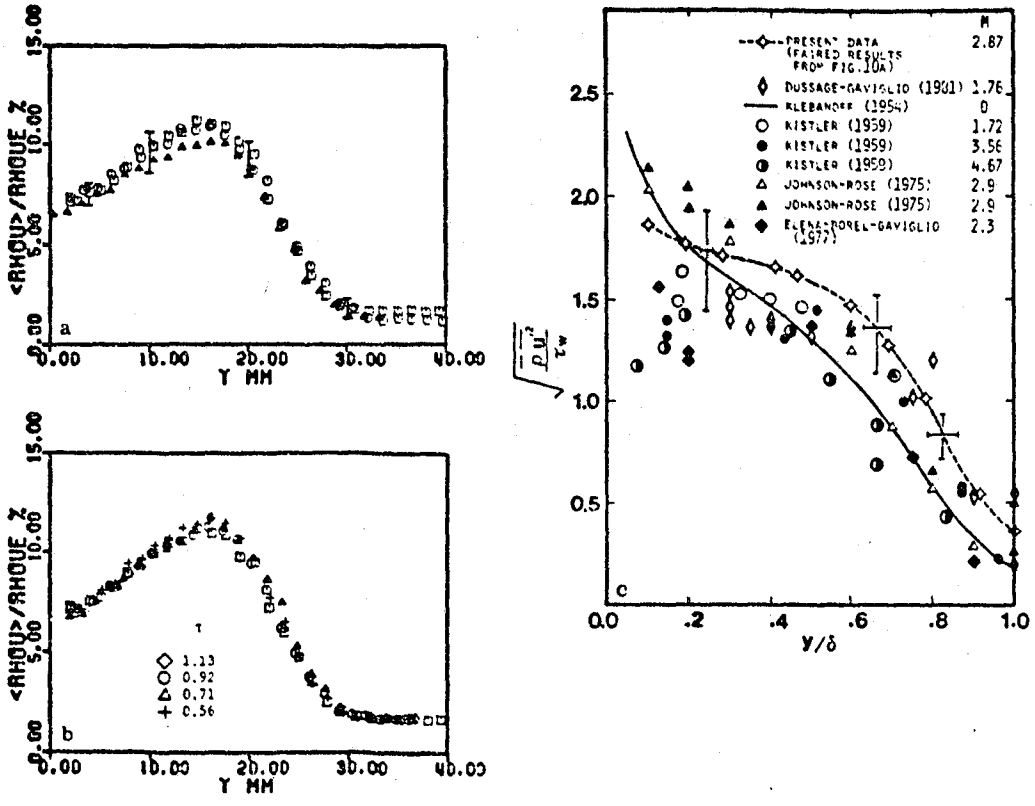

Fig. 5 a–c. a rms mass-flow fluctuation intensity for zero pressure gradient $M_\infty = 2.9$ turbulent boundary layer ($R_\ell = 77{,}600$, $\delta = 26$ mm, $C_f = 0.0011$). Results are for three different wires with overheat ratio ≈ 1.0. b rms mass-flow fluctuation intensity for zero pressure gradient $M_\infty = 2.9$ turbulent boundary layer ($R_\ell = 77{,}600$, $\delta = 26$ mm, $C_f = 0.0011$). Results are for a single wire, with varying overheat ratio. c A comparison between the inferred rms velocity fluctuation intensity (deduced from the results given in Fig. 10a) and some representative data reproduced from Dussauge and Gaviglio (1981)

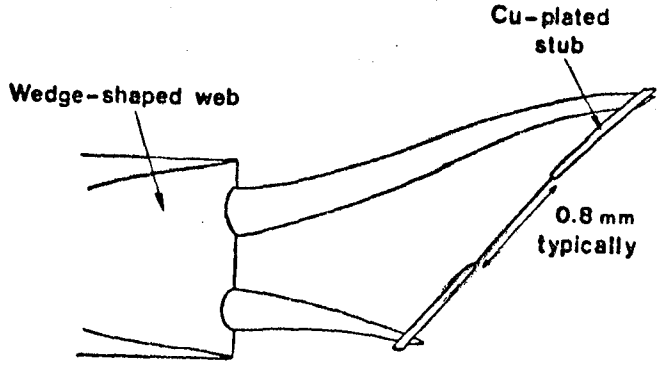

Fig. 6a A sketch of a typical inclined wire probe. The tungsten wire was 5 μm diameter.

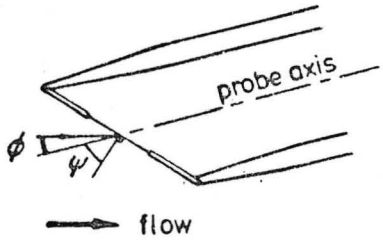

Fig. 6 b Notation for a straight inclined wire. φ is the wire angle, ψ is the yaw angle

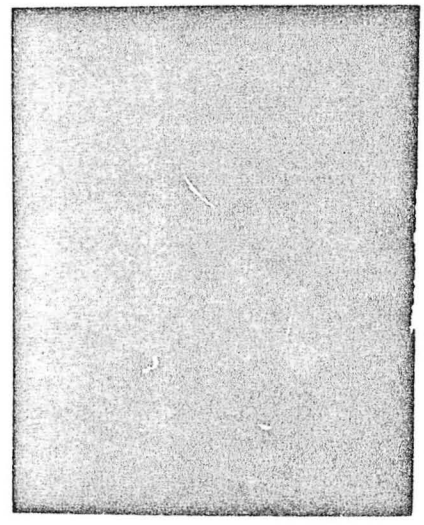

Fig. 7. Microschlieren photograph of inclined wire probe.

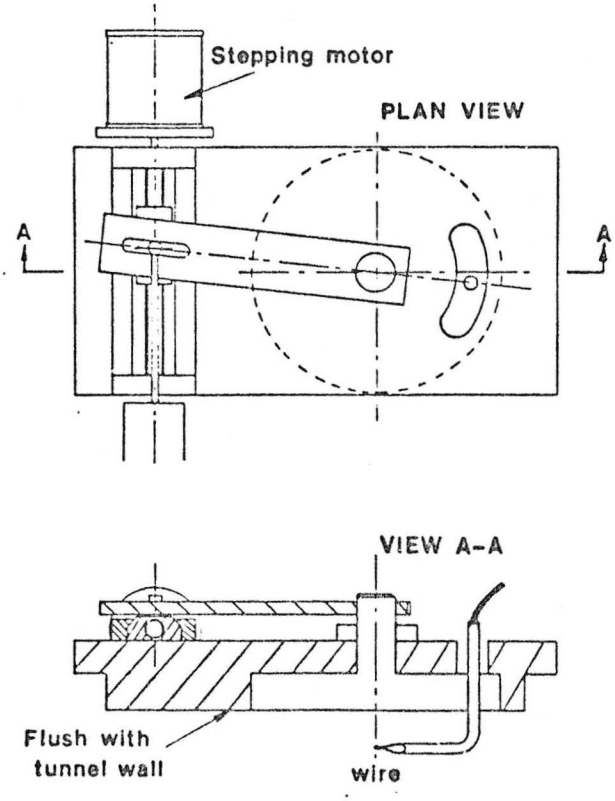

Fig. 8 Calibration device for inclined wire angle calibration.

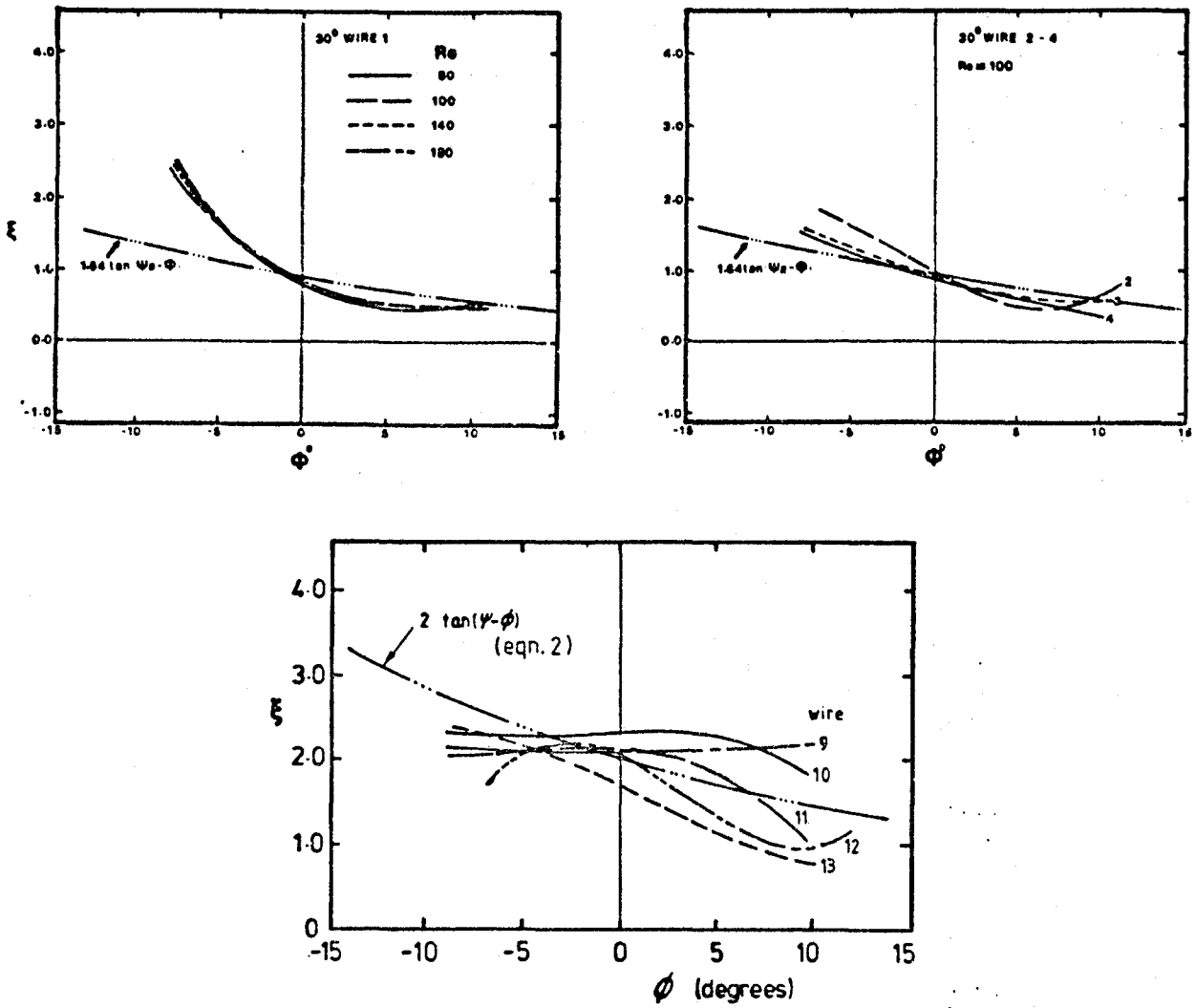

Fig. 9 Angle calibrations for various inclined wires.

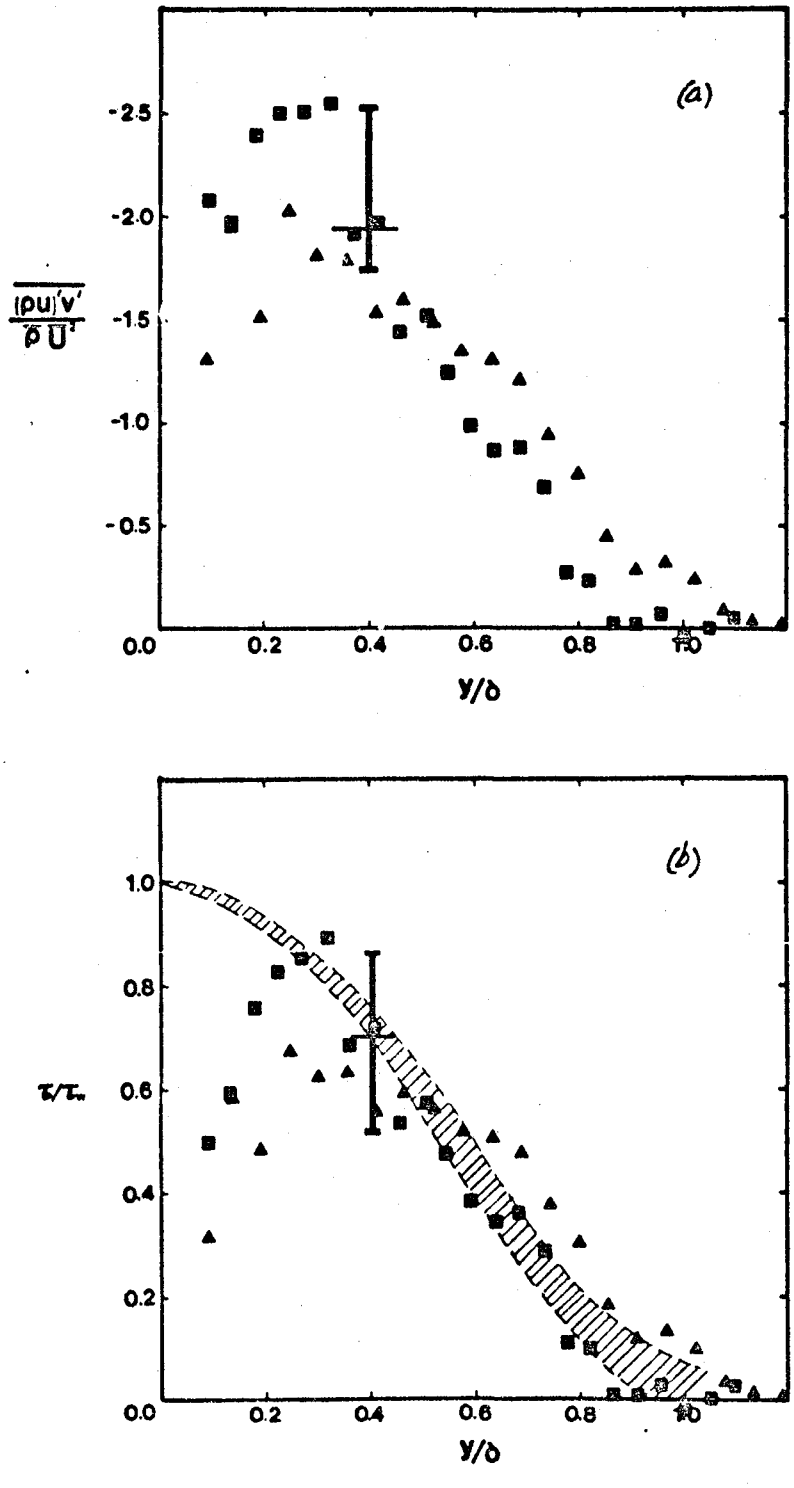

Fig. 10. Measurements of $\overline{(\rho u)'v'}$ and $\bar{\rho}\overline{u'v'}$ in a zero pressure gradient turbulent boundary layer at Mach 2.9: ■ ; 30° wire, ▲ , 45° wire. Shaded area corresponds to Sandborn's "best estimate" for the supersonic shear stress distribution (Sandborn, 1974). Error bars are only shown for the 30° wire. $(\tau/\tau_w \equiv (\bar{\rho}\,\overline{u'v'})/\rho_w u_\tau^2)$

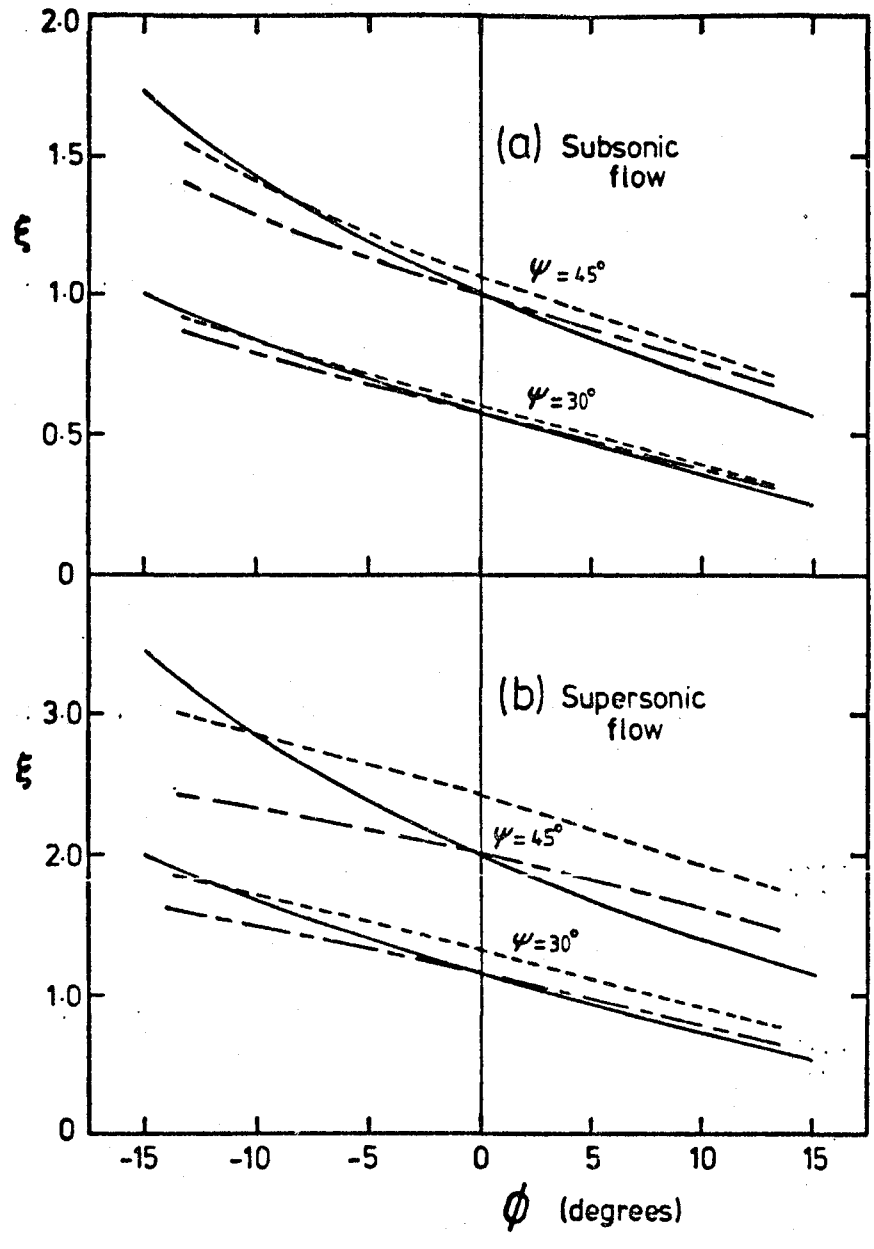

Fig. 11 Calculated results for the directional sensitivity of nominally 30° and 45° wires (ℓ = 1 mm, d = 5μm):
———— , infinitely long wire (equation 2);
——— — , straight wire with end conduction;
-------- , bowed wire with end conduction (δ = ±10)

(a) subsonic flow (Re = 4, p = 1.0), (b) supersonic flow (Re = 100, p = 2.0).

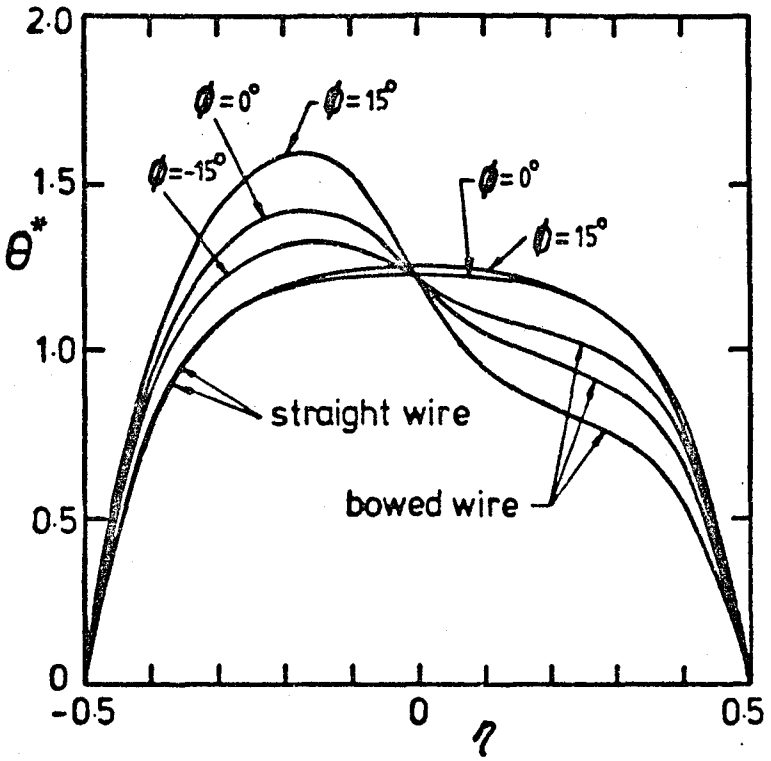

Fig. 12 Temperature distribution for nominally 45° wire in supersonic flow (ℓ = 1 mm, d = 5μm, Re = 100).

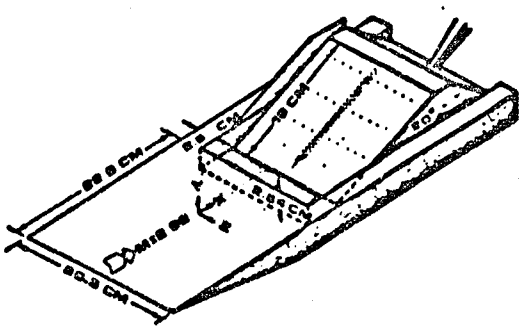

Fig. 13 Test Model.

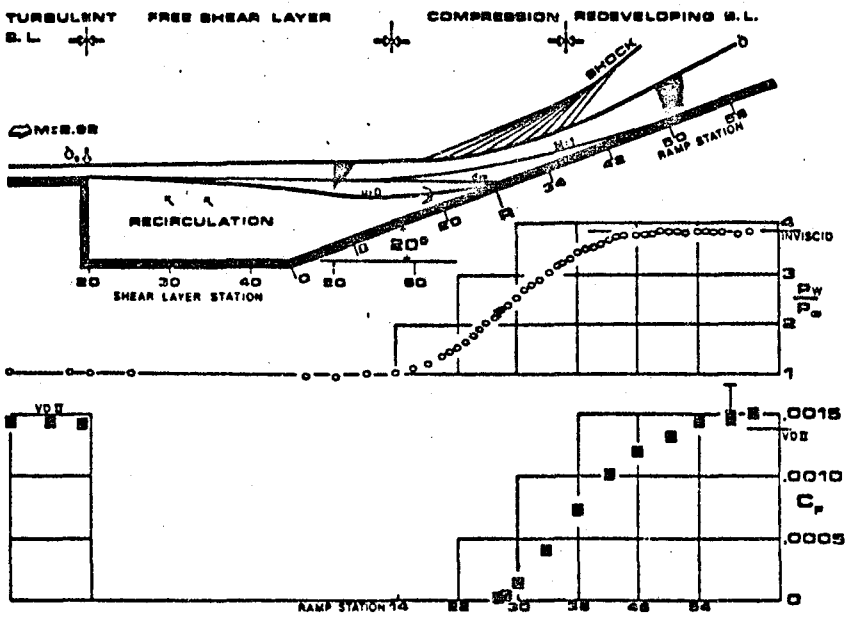

Fig. 14 Experimental Model of the Reattachment Interaction With Wall Pressure and Skin Friction Distribution.

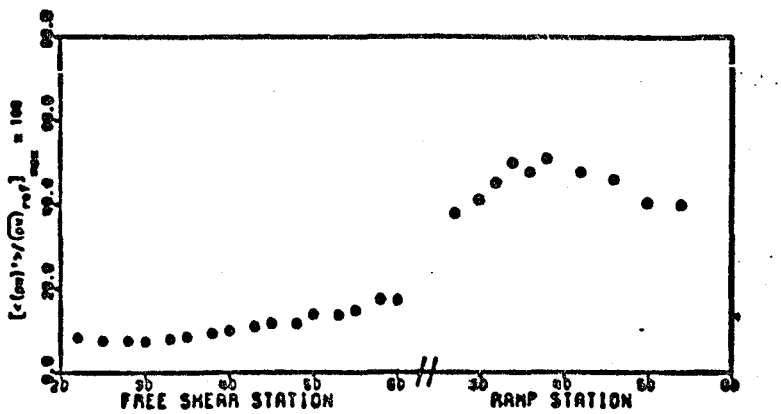

Fig. 15 Maximum Value of r.m.s. Mass-Flow Fluctuations Versus Distance Along the Flow.

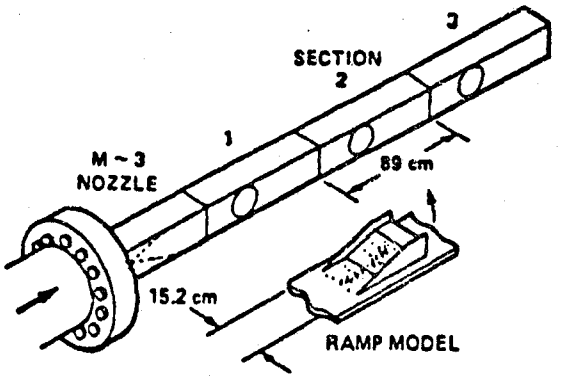

Fig. 16 Sketch of the 20 x 20 cm High Reynolds Number Channel

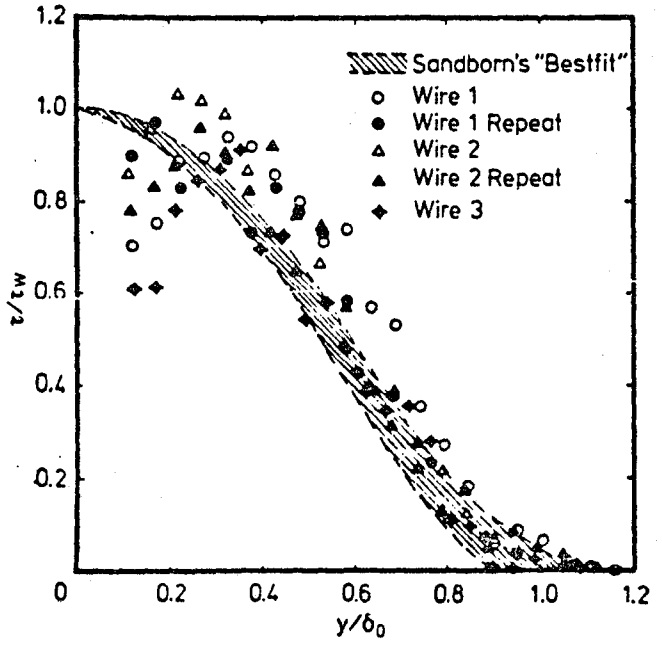

Fig. 17. Profiles of the Reynolds shear stress normalized by the surface shear stress, τ/τ_w for different wires at the upstream station ($x = -50.8$ mm).

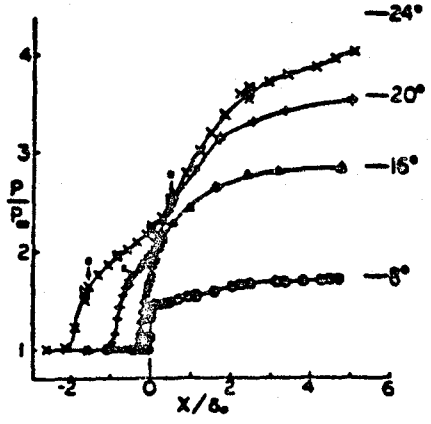

Fig. 18 Surface pressure distributions. From Settles, et al. (1979)

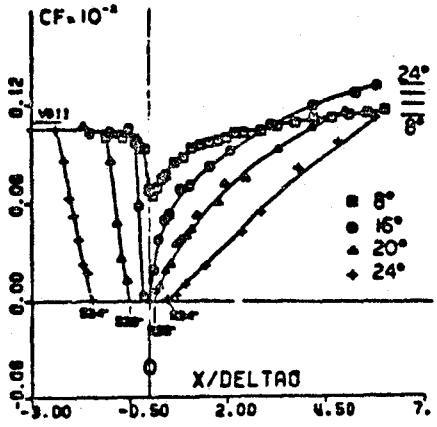

Fig. 19 Skin-friction distributions. From Settles, et al. (1979)

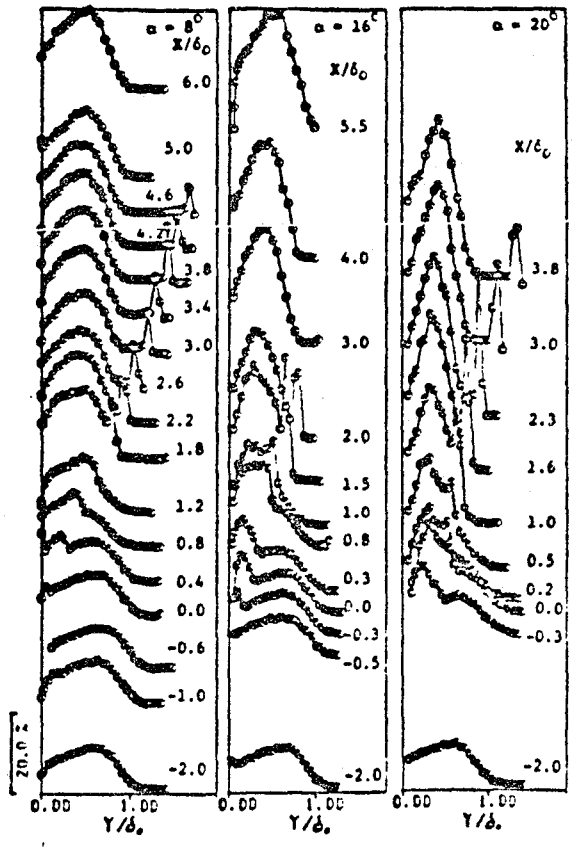

Fig. 20 Profiles of $\langle(\rho u)'\rangle/(\overline{\rho U})_{ref}$ as a function of distance normal to the wall.

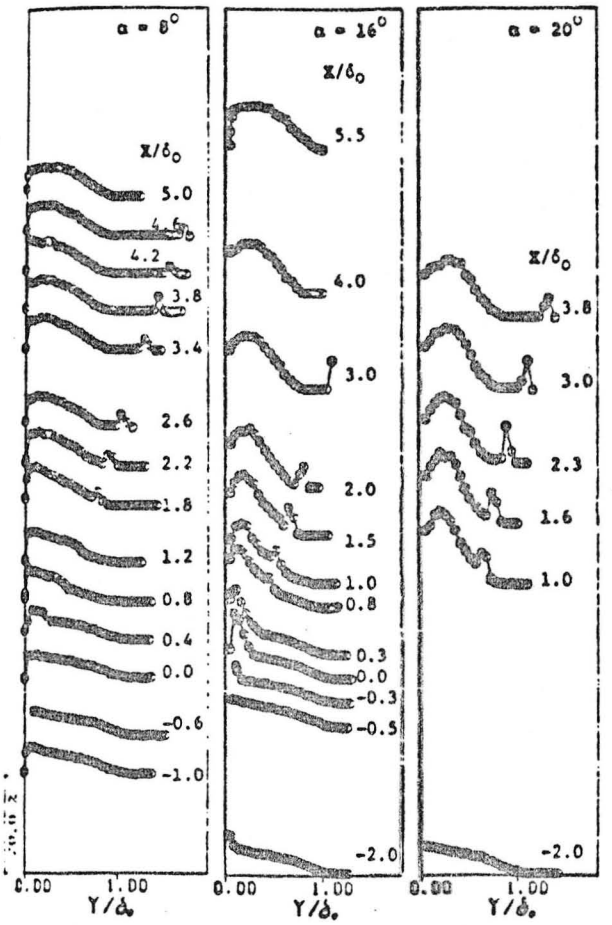

Fig. 21 Profiles of $\langle u' \rangle / \overline{U}_{ref}$ as a function of distance normal to the wall/

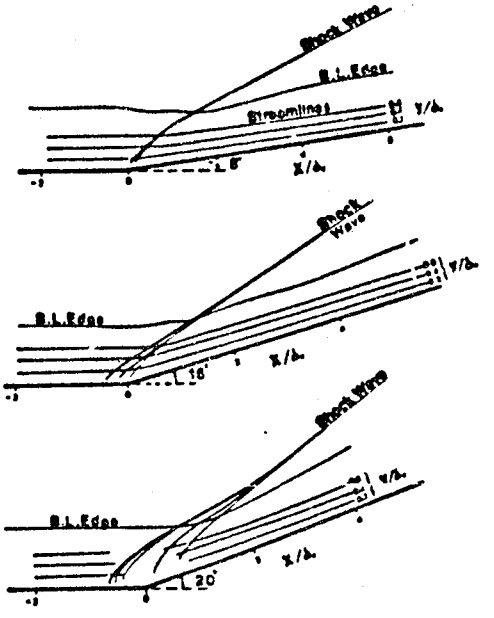

Fig. 22 Flowfield map, showing selected streamlines.

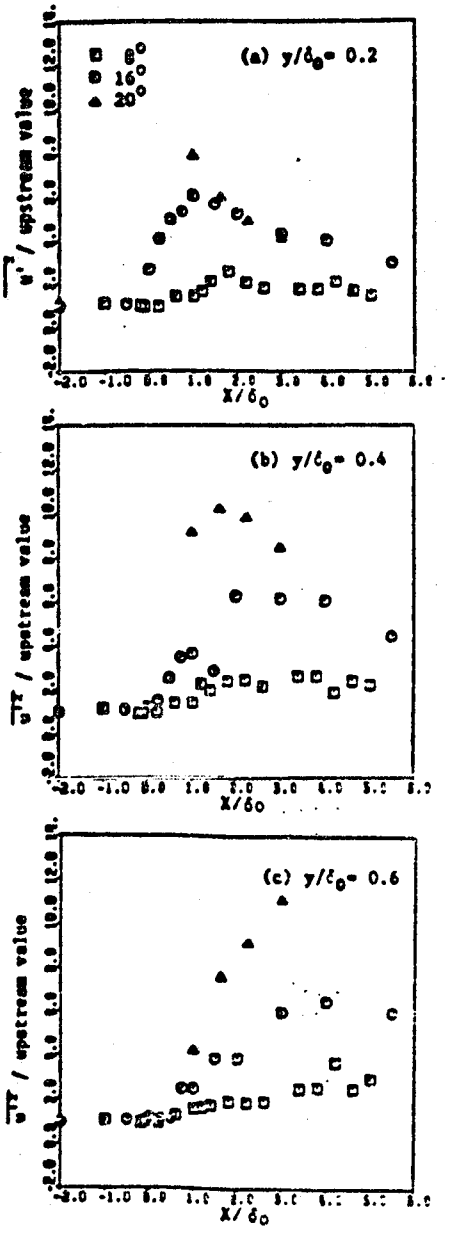

Fig. 23 Evolution of normalised $\overline{u'^2}$ along selected streamlines.

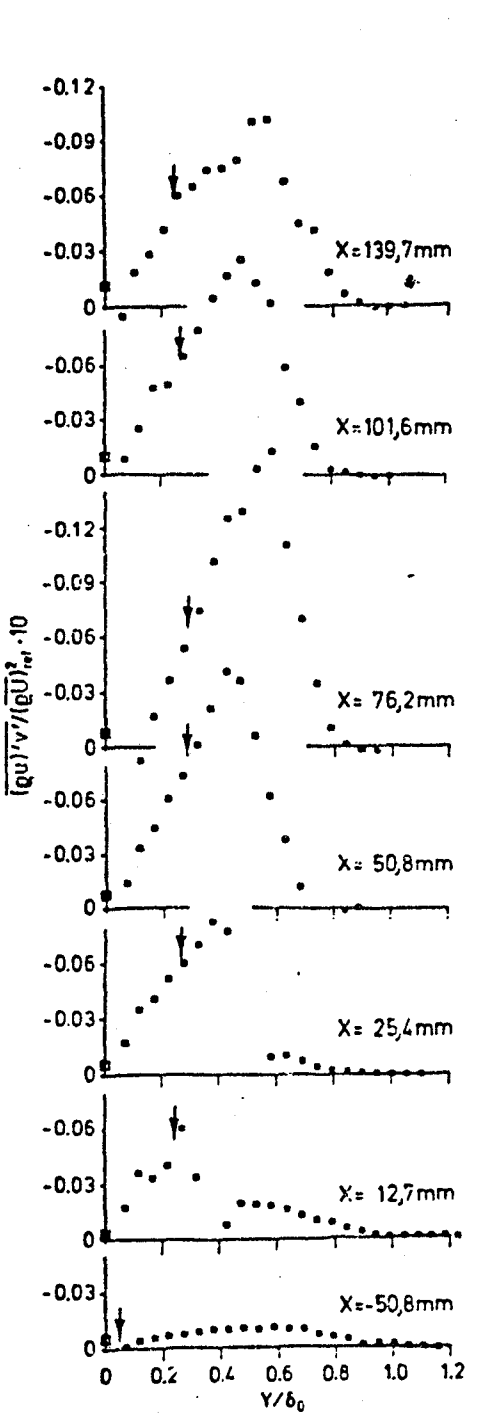

(a) 16° corner

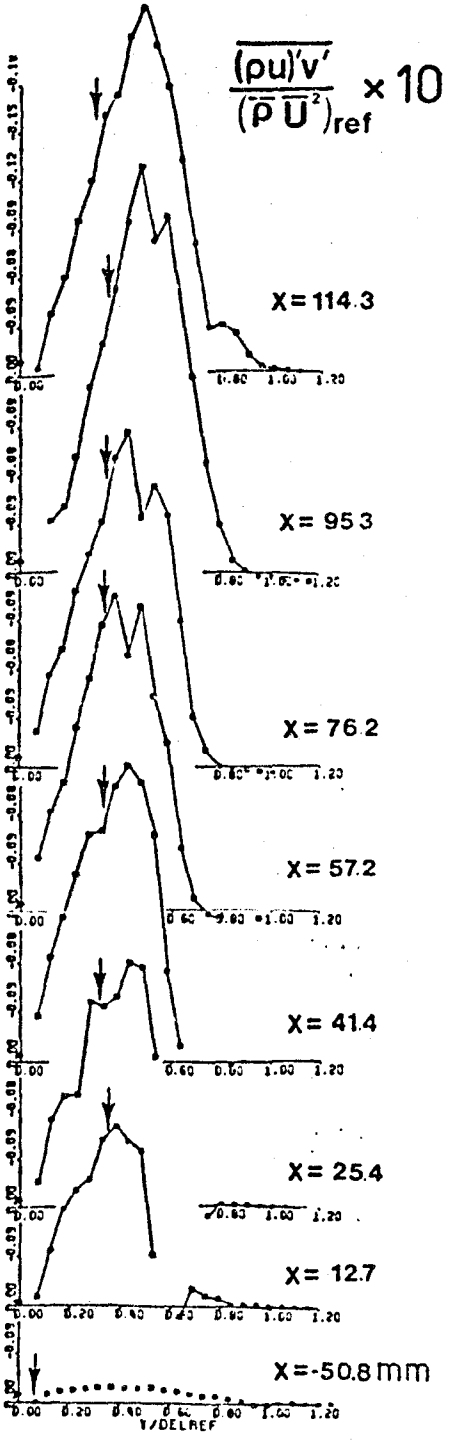

(b) 20° corner

Fig. 24 Profiles of the mass weighted Reynolds shear stress $\overline{(\rho u)'v'}/(\rho U^2)_{ref}$. The arrows indicate the locations at which the mean local *normal* Mach number is 1.2. The values given at $y = 0$ were taken from the mean flow data

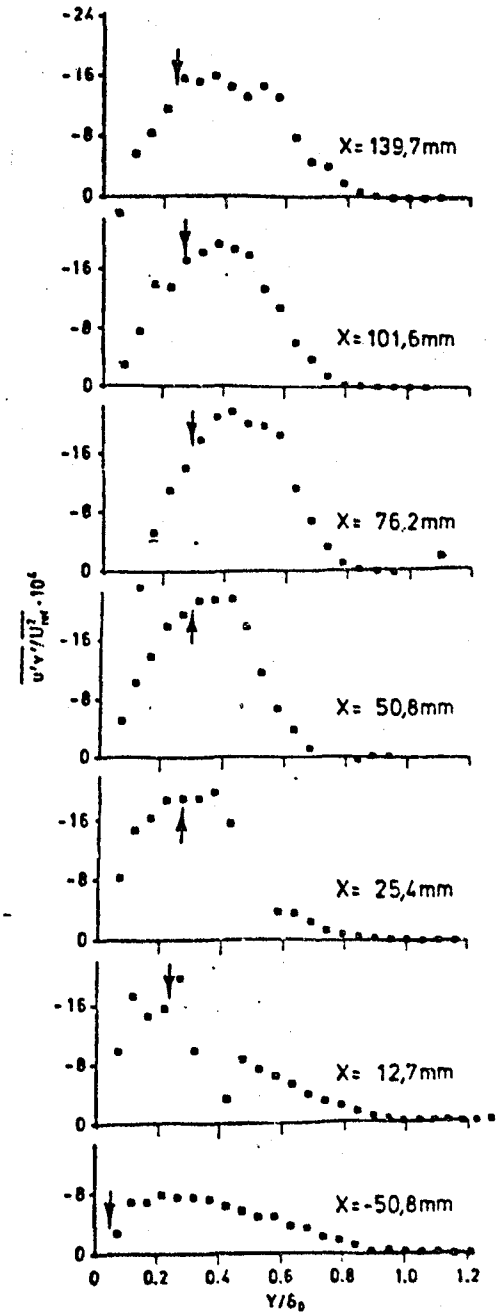

(a) 16° corner

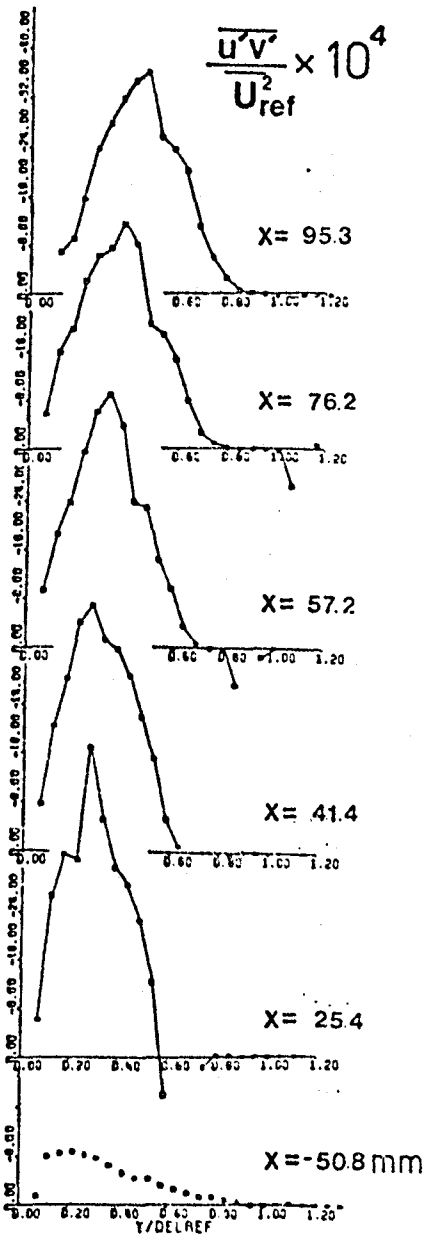

(b) 20° corner

Fig. 25. Profiles of the kinematic shear stress $(\overline{u'v'})/U_{ref}^2$. The arrows indicate the locations at which the mean local *normal* Mach number is 1.2

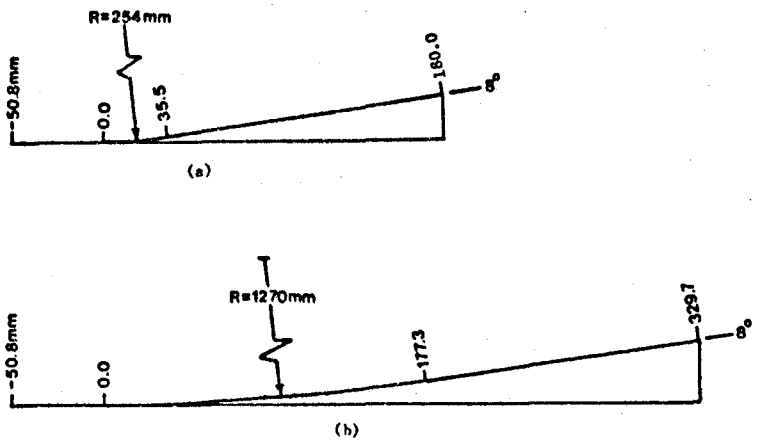

Fig. 26 Test model geometries, (a) Model I, (b) Model II

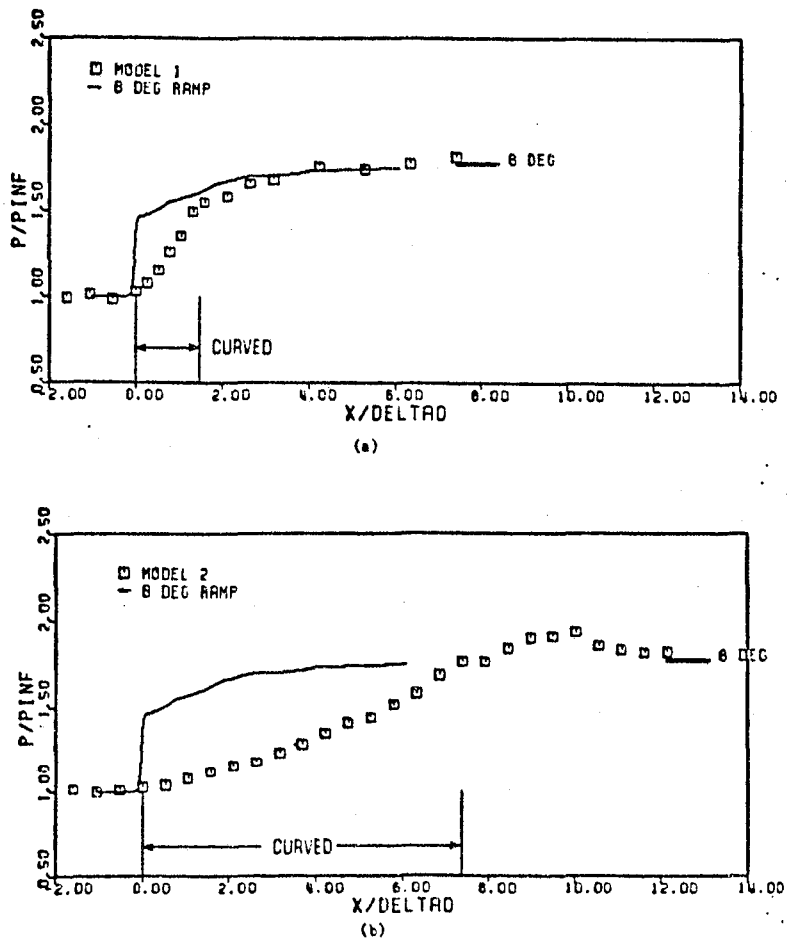

Fig. 27 Surface pressure distributions for a) Model 1, b) Model 2

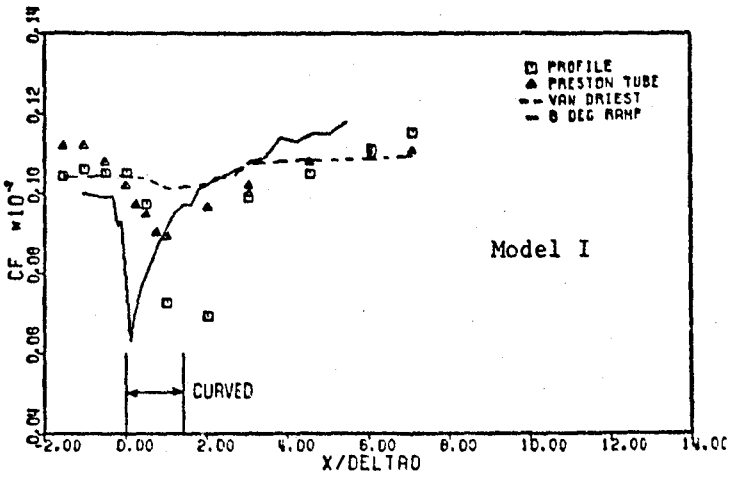

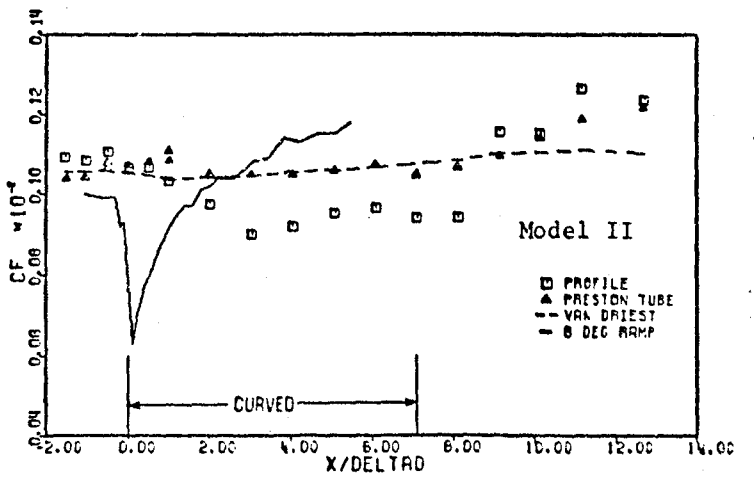

Fig. 28 Skin friction coefficient distributions for Models I and II

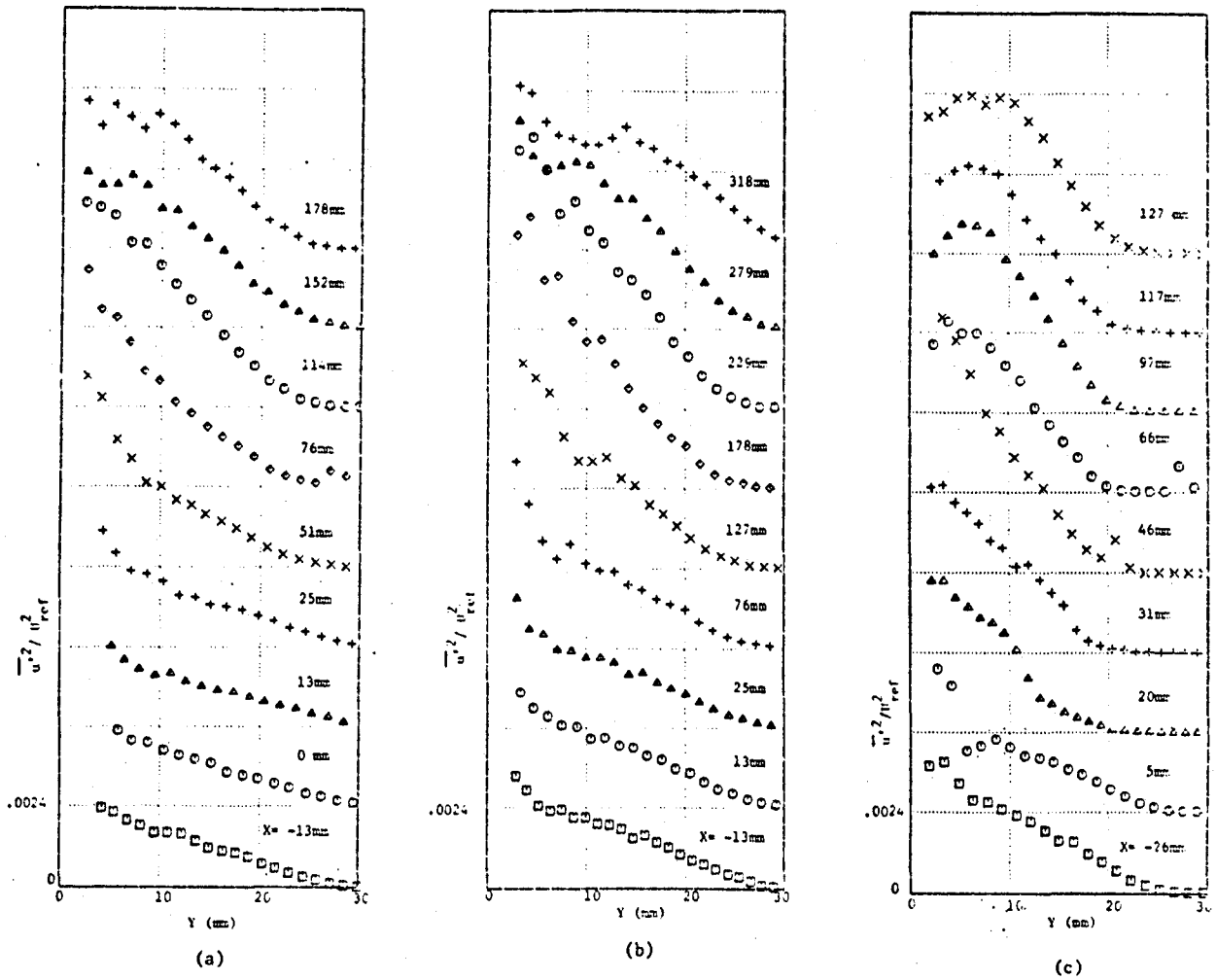

Fig. 29 Longitudinal velocity fluctuation intensity
(a) Model I (b) Model II (c) 8° corner

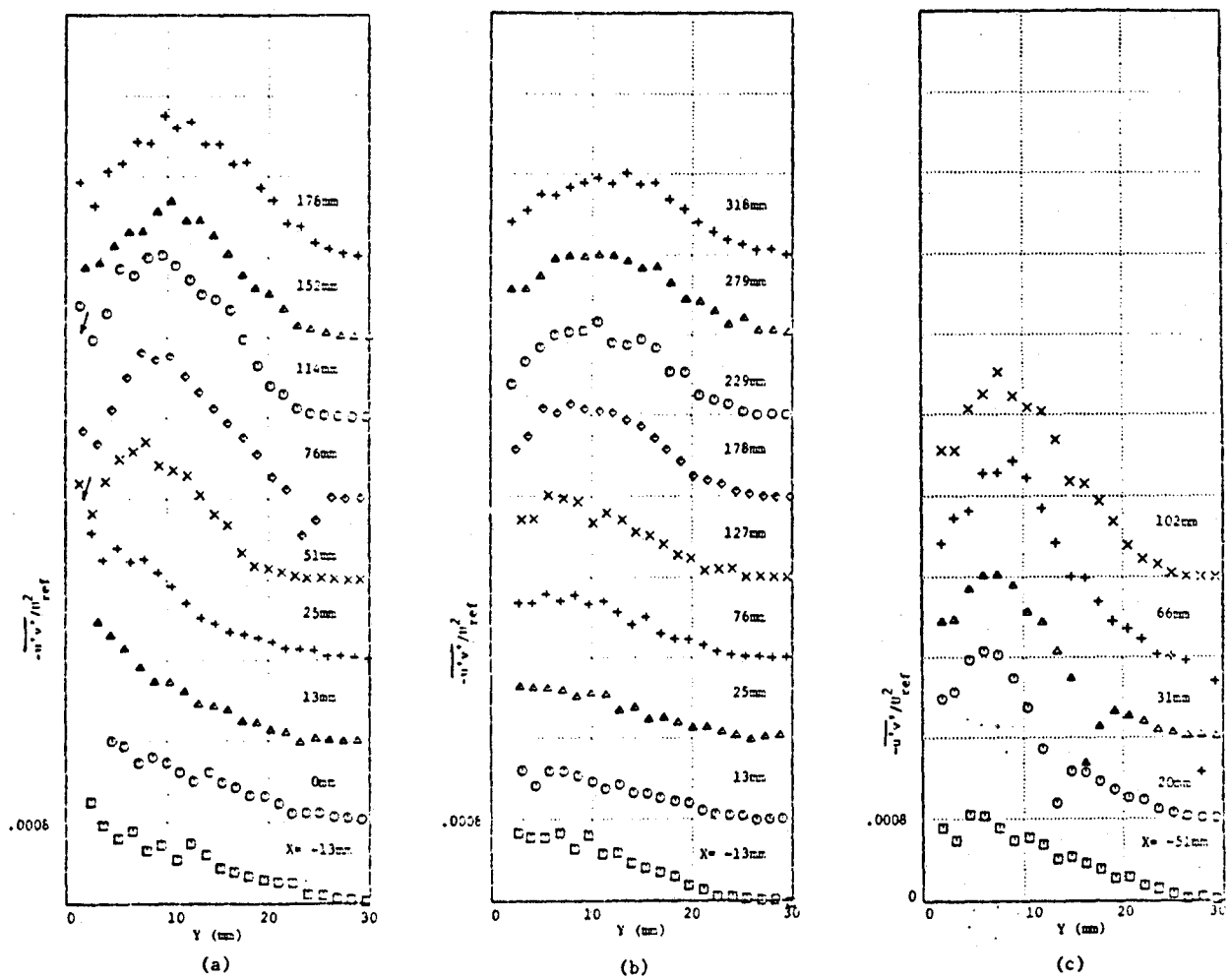

Fig. 30 Kinematic Reynolds shear stress
(a) Model I (b) Model II (c) 8° corner

Appendix A:

Publications produced under sponsorship of NAGW-240

[1] Hayakawa, K., Smits, A. J., and Bogdonoff, S. M., "Hot-Wire Investigation of an Unseparated Shock-Wave/Turbulent Boundary Layer Interaction," AIAA Paper No. 82-0985, Third AIAA/ASME Joint Thermophysics, Fluids, Plasma Heat Transfer Conference, St. Louis, Missouri, June 1982. AIAA Journal, 1984, 22:579-585.

[2] Hayakawa, K., Smits, A. J. and Bogdonoff, S. M., "Turbulence Measurements in Two Shock-Wave/Shear-Layer Interactions," Proceedings of the I.U.T.A.M. Symposium on the Structure of Complex Turbulent Shear Flow, Marseille, August-September, 1982. Published by Springer-Verlag, 1983.

[3] Smits, A. J., Muck, K. C. and Hayakawa, K., "Constant Temperature Hot-Wire Anemometer Practice in Supersonic Flows. Part I - The Normal Wire," AIAA Paper 83-0050, AIAA 21st Aerospace Sciences Meeting, Reno, Nevada, January 1983.

[4] Smits, A. J. and Muck, K. C., "Constant-Temperature Hot-Wire Anemometer Practice in Supersonic Flows. Part II - The Inclined Wire," AIAA Paper 83-0508, AIAA 21st Aerospace Sciences Meeting, Reno, Nevada, January 1983.

[5] Hayakawa, K., Smits, A. J. and Bogdonoff, S. M., "Turbulence Measurements in a Compressible Reattaching Shear Layer," AIAA Paper 83-0299, AIAA 21st Aerospace Sciences Meeting, Reno, Nevada, January 10-13, 1983. To be published, AIAA Journal, 1984.

[6] Smits, A. J., Muck, K. C. and Hayakawa, K., "Constant-Temperature Hot-Wire Anemometer Practice in Supersonic Flows. Part I - The Normal Wire," Experiments in Fluids, V1, pp. 83-92, 1983. This paper is a revised and expanded version of AIAA Paper 83-0050 (publication #3).

[7] Smits, A. J. and Muck, K. C., "Constant-Temperature Hot-Wire Anemometer Practice in Supersonic Flows. Part II - The Inclined Wire," Experiments in Fluids, V2, pp. 33-41, 1984. This paper is a revised and expanded version of AIAA Paper 83-0508 (publication #4).

[8] Smits, A. J., "Hot-Wire Anemometry," Princeton University Gas Dynamics Laboratory Internal Memorandum #51, 1983.

[9] Hayakawa, K. and Smits, A. J., "Compilation of Turbulence Data for an 8° Compression Corner at Mach 2.9, Normal Wire Data," Princeton University, Dept. of Mechanical and Aerospace Engineering, Report #1600, 1983.

[10] Hayakawa, K. and Smits, A. J., "Compilation of Turbulence Data for a Compressible Reattaching Shear Layer," Princeton University, Dept. of Mechanical and Aerospace Engineering, Report #1601, 1983.

[11] Smits, A. J., "The Static Response of a Bowed Inclined Hot Wire," to be published, Experiments in Fluids, 1984.

[12] Muck, K. C. and Smits, A. J., "The Behavior of a Compressible Turbulent Boundary Layer Under Incipient Separation Conditions," Proceedings of the Fourth Symposium on Turbulent Shear Flows, Karlsruhe, September, 1983, pp. 2.15-2.20. To be published, Springer-Verlag, 1984.

[13] Hayakawa, K., Muck, K. C., Smits, A. J. and Bogdonoff, S. M., "The Evolution of Turbulence in Shock-Wave/Boundary Layer Interactions," Proc. of the Eighth Australasian Fluid Mechanics Conference, Newcastle, Australia, December, 1983.

[14] Muck, K. C., Hayakawa, K. and Smits, A. J., "Compilation of Turbulence Data for a 16° Compression Corner at Mach 2.9," Princeton University, Dept. of Mechanical and Aerospace Engineering, Report #1619, 1983.

[15] Hayakawa, K., Muck, K. C. and Smits, A. J., "Compilation of Turbulence Data for a 20° Compression Corner at Mach 2.9," Princeton University, Dept. of Mechanical and Aerospace Engineering, Report #1620, 1983.

[16] Taylor, M. W. and Smits, A. J., "The Effect of a Short Region of Concave Curvature on a Supersonic Turbulent Boundary Layer," AIAA Paper 84-0169, AIAA 22nd Aerospace Sciences Meeting, Reno, Nevada, January 1984.

[17] Muck, K. C., Smits, A. J. and Hayakawa, K., "Behavior of a Turbulent Boundary Layer Subjected to a Shock-Induced Separation," AIAA Paper 84-0097, AIAA 22nd Aerospace Sciences Meeting, Reno, Nevada, January 1984.

[18] Gibson, R., Muck, K. C. and Smits, A. J., "Micro-Schlieren Photography of Hot-Wire Probes in Supersonic Flow," under preparation.

[19] Muck, K. C. and Smits, A. J., "The Effect of Shock Strength on Shock-Wave/Turbulent Boundary-Layer Interactions," under preparation.

[20] Muck, K. C., Spina, E. and Smits, A. J., "Compilation of Turbulence Data for an 8° Compression Corner at Mach 2.9," Princeton University, Dept. of Mechanical and Aerospace Engineering, Report #1642, 1984.

[21] Smits, A. J. and Wood, D. H., "The Response of Turbulent Boundary Layers to a Sudden Perturbation," to appear in Annual Review of Fluid Mechanics, V17, 1985. Presently available as Princeton University, Dept. of Mechanical and Aerospace Engineering, Report #1648, 1984.

[22] Taylor, M. W., "The Response of a Supersonic Turbulent Boundary Layer to Compression and Curvature," M.Sc. Thesis, Dept. of Mechanical and Aerospace Engineering, Princeton University, June 1984.

In addition to the above publications, the following presentations were made at the American Physical Society meetings in 1982 and 1983:

Hayakawa, K., Smits, A. J. and Bogdonoff, S. M., "Compressive Effects on Turbulence through Supersonic Reattachment," Bulletin of the American Physical Society, Vol. 27, 1982, p. 1180.

Smits, A. J., Muck, K. C. and Hayakawa, K., "Calibrating an Inclined Hot-Wire for Measurements in a Supersonic Flow," Bulletin of the American Physical Society, Vol. 27, 1982, p. 1199.

Muck, K. C. and Smits, A. J., "The Behavior of Turbulence in Shock-Wave/Boundary-Layer Interactions," Bulletin of the American Physical Society, Vol. 28, 1983, p. 1359.

END

DATE

FILMED

FEB 7 1985